A Parameterization of the Cloudiness Associated with Cumulus Convection; Evaluation Using TOGA COARE Data

SANDRINE BONY AND KERRY A. EMANUEL

Program for Atmospheres, Oceans and Climate, Massachusetts Institute of Technology, Cambridge, Massachusetts

(Manuscript received 28 February 2000, in final form 17 April 2001)

ABSTRACT

A new parameterization of the cloudiness associated with cumulus convection is proposed for use in climate models. It is based upon the idea that the convection scheme predicts the local concentration of condensed water (the in-cloud water content) produced at the subgrid scale, and that a statistical cloud scheme predicts how this condensed water is spatially distributed within the domain. The cloud scheme uses a probability distribution function (PDF) of the total water whose variance and skewness coefficient are diagnosed from the amount of condensed water produced at the subgrid scale by cumulus convection and at the large scale by supersaturation, from the degree of saturation of the environment, and from the lower bound of the total water distribution that is taken equal to zero.

This parameterization is used in a single-column model forced by the Tropical Ocean Global Atmosphere Coupled Ocean–Atmosphere Response Experiment (TOGA COARE) data, and including the cumulus convection scheme of Emanuel whose humidity prediction has been optimized using these data. Simulations are carried out during the 120 days of operation of the TOGA COARE intensive observation period. The model is able to reproduce some of the main characteristics of the cloudiness observed over the warm pool. This includes the occurrence of different populations of clouds (shallow, midlevel, and deep convective), a minimum cloud cover between 600 and 800 hPa, some relationship between the distribution of cloud tops and the presence of stable atmospheric layers, the formation of long-lasting upper-tropospheric anvils associated with the maturation of the convective cloud systems, and the presence of an extensive layer of thin cirrus clouds just below the tropopause. Nevertheless, shallow-level clouds are likely to be underestimated. The behavior of the predicted cloud fields is consistent with some statistical features suggested by cloud-resolving model simulations of tropical cloud systems over oceans. The radiative fluxes calculated interactively by the model from the predicted profiles of humidity, temperature, and clouds are in reasonable agreement with satellite data. Sea surface temperatures predicted by the model using its own radiative and turbulent fluxes calculated at the ocean surface differ from observations by a few tenths of a degree.

Sensitivity tests show that the performance of the cloudiness parameterization does not critically depend upon the choice of the PDF. On the other hand, they show that the prediction of radiative fluxes is improved when the statistical moments of the PDF are predicted from both large-scale variables and subgrid-scale convective activity rather than from large-scale variables only.

1. Introduction

Observational, theoretical, and numerical studies have pointed to the radiative effects of clouds as an important forcing of large-scale atmospheric circulations and ocean–atmosphere interactions. This confers to these effects an important role in natural climate variability (e.g., diurnal variations, intraseasonal oscillations, interannual variations) and in the sensitivity of climate to external perturbations.

Cloud radiative effects are particularly important in tropical regions, where deep convection produces extensive and deep upper tropospheric stratiform clouds (anvils). The large horizontal extent (several hundred kilometers in length) and longevity (up to one day) of these clouds (Chen and Houze 1997) make them interact very efficiently with radiation. Recent experiments also reveal the presence over warm ocean regions of an abundant population of midlevel clouds that may also modulate the radiative heating of the troposphere (Johnson et al. 1999). By transporting water vapor from the surface to upper atmospheric levels, cumulus convection constitutes one mechanism by which cloud particles are produced. In the Tropics, over midlatitude continents in summer or over midlatitude oceans in winter, convection is likely to be the primary source of clouds.

To predict the radiative effects of clouds, two fundamental cloud properties must be known: the cloud fractional area and the cloud water content. The first one determines the relative areas of the clear-sky and

Corresponding author address: Sandrine Bony, LMD/CNRS, UPMC, Case Courier 99, 4 place Jussieu, 75252 Paris Cedex 05, France.
E-mail: bony@lmd.jussieu.fr

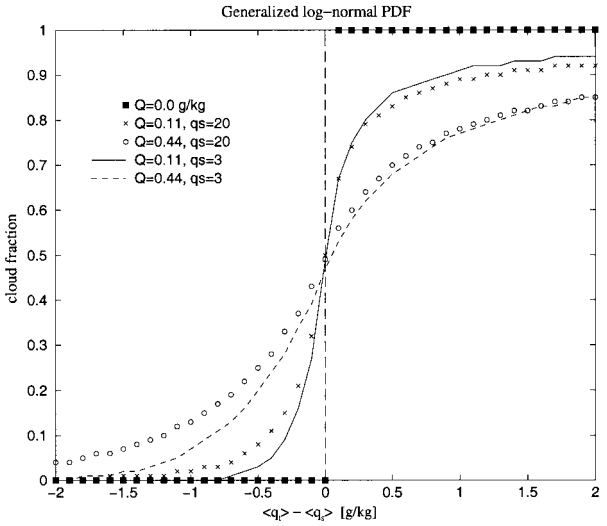

FIG. 1. Cloud fraction vs the saturation deficit (or excess) defined as $\overline{q}_t - \overline{q}_s$ computed by the cloud scheme using a generalized log-normal PDF. Results are shown for different values of the subgrid-scale condensate mixing ratio ($Q = q_c^{\text{in,SUB}}$, in g kg^{-1}) and for different values of the saturation mixing ratio $\overline{q}_s$ (in g kg^{-1}), lower (larger) values of q_s being representative of the upper (lower) troposphere.

cloudy parts of a large-scale domain (or a model grid-box), and the second one is required to predict, with some information about the droplets size distribution and absorption coefficients of radiation, the cloud emissivity, and the cloud optical thickness or albedo. As discussed by Randall (1989), cloud microphysical processes (e.g., precipitation) and cloud optical properties both depend on the *local* concentration of cloud water, which is basically the domain-averaged cloud water content divided by the cloud fraction. This makes the prediction of the cloud fraction particularly critical for the simulation of the latent heating and radiative effects of clouds.

The prediction of cloud fraction in climate models is a difficult task, however. An important reason is that most clouds are produced by condensation processes that take place at spatial scales much smaller than the size of a model grid box (which is typically a few hundred kilometers in length). This is the case in particular for clouds produced by cumulus convection, planetary boundary-layer turbulence, gravity waves, or orographic lifting. One has therefore to parameterize these clouds as functions of the prognostic variables explicitely resolved by the model, without losing information about the physical processes that occur at the subgrid scale and that are responsible for these clouds. In tropical regions experiencing deep convection for instance, observational studies show that the time evolution of the cloud cover is closely tied to the life cycle of individual convective systems (Chen and Houze 1997).

Cloudiness parameterizations used in climate models can be classified into two main categories. The first one, referred to as diagnostic or semiempirical schemes, predicts the subgrid-scale cloud fraction as a function of large-scale predictors such as the mean relative humidity (e.g., Slingo 1980). However, cloud resolving model (CRM) simulations show that the mean relative humidity is a poor predictor of the upper level cloudiness in convective regions (Xu and Randall 1996a, hereafter referred to as XR96a). As stressed by Randall (1989), upper-tropospheric stratiform clouds associated with deep convection are likely to be better represented by using condensed water variables as additional predictors. XR96a proposed such a parameterization, using the grid-averaged mixing ratio of condensate as the primary predictor, and the grid-averaged relative humidity as a secondary predictor. Some climate models use prognostic equations for cloud condensate and introduce in these equations subgrid-scale source or sink terms linked to cumulus detrainment (e.g., Tiedtke 1993; Ose 1993; Zender and Kiehl 1994; Del Genio et al. 1996; Fowler et al. 1996). In such models, the coupling between the representations of the cloudiness and of cumulus convection may be achieved by using the grid-averaged mixing ratio of condensate as a predictor of the cloud fraction. The second family of cloudiness parameterizations is referred to as statistical schemes. These schemes represent the subgrid-scale variability of conserved variables by a probability distribution function (PDF) whose shape and width have to be specified. Xu and Randall (1996b, hereafter referred to as XR96b), presented a detailed evaluation of these schemes and showed that in convective regions the calculation of the PDF moments relies on assumptions that are not supported by CRM simulations. Recently, Tompkins (2001, manuscript submitted to *J. Atmos. Sci.*) proposed a statistical cloud parameterization that predicts the effects of deep convection and vertical turbulence upon the moments of the total water PDF. The purpose of the present study is to propose and to evaluate against observations a new statistical cloud parameterization that links both the cloud water content and the cloud fraction to the convective activity parameterized by the convection scheme of Emanuel (Emanuel 1991; Emanuel and

TABLE 1. Parameter values used in this study that differ from those of Emanuel and Zivkovic-Rothman (1999).

Parameter	Description	Old value	New value
Λ	Mixing parameter	0.06 mb^{-1}	1.5 mb^{-1}
σ_s	Fraction of rain shaft falling through environment	0.15	0.12
ΔT_k	Convection buoyancy threshold	0.65 K	0.90 K
$\epsilon_{\max}$	Maximum precipitation efficiency	1.000	0.999

Zivkovic-Rothman 1999), and that fulfills some of the main requirements suggested by CRMs in convective regions.

A difficulty that hindered the development and improvement of cloud cover parameterizations is the lack of evaluation data. Current available satellite data do not provide much information about the vertical distribution of clouds, and observational estimates of the cloud water content remain quite uncertain. Field experiments such as the Global Atmospheric Research Program's Atlantic Tropical Experiment (GATE) or the Tropical Ocean and Global Atmosphere Coupled Ocean–Atmosphere Response Experiment (TOGA COARE) provide lots of data about thermodynamical fields that may be used to evaluate some parameterizations used in the models (e.g., Emanuel and Zivkovic-Rothmann 1999; Sud and Walker 1999), but they do not provide reliable data about clouds, in particular their fractional area and water content, nor the large-scale advection of condensed water. On the modeling side, CRMs provide invaluable information about the qualitative behaviour of clouds associated with convection, that may be used as guidance for cloud parameterizations (e.g., Xu and Krueger 1991; XR96b). However, cloud microphysics still has to be parameterized in these models, and CRM simulations are sensitive to their representation (e.g., Wu et al. 1999). The assumption made in this study, however, is that the combined use of all these sources of information about the behaviour of clouds in regions experiencing convection allows us to evaluate a cloud scheme in a sufficiently stringent and rigorous manner.

Radiative fluxes constitute one of the most reliable observations against which a cloud parameterization can be tested. However, for this to be true, errors in the temperature and water vapor fields predicted by the model must not affect too much the performance of the cloud scheme. Hence, the strategy adopted in this study is to use our cloud parameterization in a single-column model forced by TOGA COARE data and whose water vapor and temperature predictions have been previously optimized against these data.

This paper is organized as follows: In the next section, the design of the cloud scheme is presented. Section 3 presents simulations performed by including this parameterization in a single-column model using a convection scheme that has been optimized in its water vapor prediction. Section 4 presents qualitative and quantitative evaluations of the cloud fields produced in these simulations. We 1) assess the radiative fluxes calculated by the model against observations; 2) test the ability of the model to predict sea surface temperatures using its own radiative, latent, and sensible heat fluxes calculated at the ocean surface; 3) verify that the cloudiness parameterization reproduces some of the main statistical features of tropical cloud systems suggested by CRM simulations; and 4) check the consistency of the predicted cloud fields with observations made over the warm pool. Section 5 investigates the sensitivity of the radiation simulated by the model to the two main original features of the present scheme, namely the type of PDF used to represent the subgrid-scale variability, and the choice of the predictors of the statistical moments of the PDF. Section 6 gives a summary and a conclusion of the study.

2. Cloudiness parameterization

a. The approach

The cloud water content is related to the amount of condensation that takes place within a domain. The cloud fraction determines how this condensed water is spatially distributed within this domain.[1] To predict the subgrid cloud amount and cloud water consistent with the representation of the subgrid-scale processes, the main feature of our approach is to consider that *the parameterization of the subgrid-scale condensation process* (e.g., the convection scheme) should *predict the in-cloud water content,* while *a statistical cloud scheme should predict how this cloud water is spatially distributed within the domain.* This differs from traditional approaches that make the cloud scheme predict both the domain-averaged cloud water content and the cloud fraction. With our approach, the main natural predictors of the subgrid cloud fraction are the amount of condensate produced at the subgrid-scale and/or at the large-scale and the degree of saturation of the large-scale environment. The in-cloud water content, which depends on the microphysical processes that take place within the convective systems (condensation, precipitation, evaporation, and turbulent mixing with environmental air) and at the large-scale, is a predictor of the cloud fraction and of the cloud optical properties. It guarantees therefore a tight coupling between the dynamics of clouds (in particular the evolution of the convective activity) and the radiative effects of clouds.

Our intent is to develop a cloudiness representation that is coupled with the convection scheme originally developed by Emanuel (1991) and subsequently modified and optimized by Emanuel and Zivkovic-Rothman (1999). This scheme is a stationary model of convection based on the episodic mixing model of Raymond and Blyth (1986) and using a subcloud-layer quasi-equilibrium closure. It predicts the effects of the convective systems upon the large-scale profiles of temperature and humidity without partitioning explicitly the relative contributions of the convective and stratiform parts of the system. Indeed, unlike other convection schemes, in particular the Arakawa–Schubert (1974) scheme, this convection scheme provides an idealized model of the collective effect of an ensemble of individual O(100m)-

[1] The term ''subgrid-cloud fraction'' should actually be understood as a ''subgrid cloud volume.'' Nevertheless, we will hereafter refer to this term as if it was an actual horizontal area.

scale updrafts and downdrafts of different intensities, that compose the convective systems. It is thus intended to represent thermodynamically the whole system and not only the convective core–cells of the system. Moreover, due to the above feature and to the boundary layer quasi-equilibrium closure, the convective activity is represented in time in a continuous way. This is in contrast with a more ''triggering-based approach'' used in some other convection schemes. Therefore, the statistical representation of the convective activity by the Emanuel scheme is continuously modulated by the large-scale forcing, and does not exhibit ''switching'' behavior. These particularities of the convection scheme enable us to consider that the vertical profile of the condensed water mixing ratio predicted by the scheme is adequate to represent the in-cloud water content of the ensemble of clouds (convective + stratiform) associated with the convective activity within the domain.

Observations show that clouds associated with scattered convection may cover only a tiny fraction of the domain, but as the convective systems mature and get organized, the cloud cover may extend to mesoscales and even up to large scales as the stratiform anvils develop. In most climate models, a distinction is made between convective and stratiform cloud amounts. The first category is considered either as negligible or set to an arbitrary value that depends empirically on variables such as the convective precipitation (Slingo 1987) or the convective mass flux (Fowler and Randall 1996). However, as noticed by Xu and Krueger (1991) and by observational studies (Houze and Betts 1981), clouds that cannot be classified in the anvil category represent a significant fraction of the cloud population in the Tropics: during the TOGA COARE experiment for instance, cumulus congestus were found to constitute over half of the precipitating convective clouds (Johnson et al. 1999). With the coupled cloud-convection scheme presented in this study, the distinction between convective and stratiform clouds is not necessary, and all types of clouds directly associated with cumulus convection may be represented a priori.

Our cloud scheme is statistical in nature and uses the total water content q_t (vapor + condensed) as a prognostic variable. Within a specified domain [a model grid-box or the intensive flux array (IFA) region of the TOGA COARE experiment], q_t is assumed to be a random variable characterized by a mean value $\overline{q}_t$ and by a subgrid-scale variability around the mean[2] described by a PDF $P(q_t)$ such that

$$\int_0^\infty P(q_t)\, dq_t = 1, \quad \text{and} \tag{1}$$

$$\mu \equiv \overline{q}_t = \int_0^\infty q_t P(q_t)\, dq_t. \tag{2}$$

The higher-order statistical moments (variance, skewness coefficient) are given by

$$\sigma^2 = \int_0^\infty (q_t - \overline{q}_t)^2 P(q_t)\, dq_t, \quad \text{and} \tag{3}$$

$$S = \left[\int_0^\infty (q_t - \overline{q}_t)^3 P(q_t)\, dq_t\right] \Big/ \sigma^3. \tag{4}$$

The cloud fraction f and the domain-averaged amount of condensate $\overline{q_{tc}}$ are obtained by integrating the PDF over the saturated domain:

$$f = \int_{q_s}^\infty P(q_t)\, dq_t, \tag{5}$$

$$\overline{q}_{t_c} = \int_{q_s}^\infty q_t P(q_t)\, dq_t. \tag{6}$$

The *in-cloud* condensed water content q_c^{in} is then given by

$$q_c^{\text{in}} = \frac{\overline{q}_{t_c}}{f} - q_s. \tag{7}$$

Note that we assume here that the temperature is horizontally homogeneous within the domain [therefore the notation q_s used in the following formulas actually means $q_s(\overline{T})$]. Indeed, the tropical atmosphere, characterized by a large Rossby radius of deformation, can not sustain significant horizontal temperature gradients on time scales greater than those associated with internal inertia-gravity waves. Besides this theoretical statement, cloud resolving model simulations confirm that considering the subgrid-scale distribution of total water fluctuations only (instead of a joint total water-liquid water potential temperature distribution) is a valid approximation in the Tropics (XR96b; Tompkins 2001, manuscript submitted to *J. Atmos. Sci.*). Ignoring subgrid-scale fluctuations of temperature may not be as legitimate in middle and high latitudes, however. This study is dealing only with tropical regions, but further studies will be necessary to quantify the error introduced by such an approximation in extratropical regions.

b. PDF

Our choice of the PDF is guided by observations and CRM simulations. Aircraft data collected in the subcloud layer suggest that the distribution of the total water fluctuations at low atmospheric levels is close to a normal distribution (Cotton and Anthes 1989). Analyzing CRM simulations of the GATE Phase III experiment,

[2] Note that one may consider the distribution of a pair of moist conservative variables (e.g., the total water and the liquid water potential temperature), as done by Sommeria and Deardorff (1977) or Smith (1990), instead of the total water only. However, XR96b showed that considering only the distribution of q_t was a reasonable approximation, owing perhaps to dynamical constraints on the level of variability of virtual temperature.

XR96b find that the PDF of q_t in regions of clouds associated with cumulus convection is close to Gaussian at low levels (700 hPa), but skewed at high levels. They show that the skewness factor depends on the scale of motions within the domain, and that in the presence of different scales of motion (as this is the case in a GCM grid box), it is positive. They also point out that the skewness varies with altitude, being more and more positive as the altitude increases. This result may be intuitively interpreted as the natural statistical consequence of the fact that q_t values are obviously always positive, and that the mean value of q_t decreases with altitude while its upper bound remains approximately equal to the subcloud specific humidity: a given subgrid-scale variance of q_t is then associated with a increasing positive skewness with altitude.[3]

In view of these results, we would like a PDF of variable skewness that may tend toward a normal distribution in certain conditions. The generalized lognormal PDF of Hosking and Wallis (1997) presents these properties (appendix A). The definition of this PDF is such that it is equivalent to a Gaussian distribution if it is not bounded, but becomes positively (negatively) skewed if it is bounded by a lower (respectively, upper) value. If X is a lower bound of the total water distribution (q_t X), the generalized lognormal PDF is characterized by three parameters (λ, α, and k) such that

$$P(q_t) = \frac{e^{ky - y^2/2}}{\alpha\sqrt{2\pi}}$$

$$y = \begin{cases} -\dfrac{1}{k}\ln\dfrac{X - q_t}{X - \lambda} & \text{for } k < 0 \\ \dfrac{q_t - \lambda}{\alpha} & \text{for } k = 0, \end{cases} \tag{8}$$

with $k = \alpha/(X - \lambda)$ by definition of the lower bound (α, $\lambda > 0$, $k < 0$). Note that $P(q_t)$ is continuous in k [the formulation of $P(q_t)$ for $k = 0$ corresponds to the limit $k \to 0$].

The PDF parameters λ, α, and k, which are functions of the mean, variance and skewness coefficient (appendix A), depend on the minimum value X of q_t:

$$k = -\sqrt{\ln\left[1 + \left(\frac{\sigma}{\mu - X}\right)^2\right]}, \tag{9}$$

$$\lambda = X + (\mu - X)e^{-k^2/2}, \quad \text{and} \tag{10}$$

$$\alpha = -k(\mu - X)e^{-k^2/2}, \tag{11}$$

k being a function of $\sigma/(\mu - X)$ and μ decreasing with altitude, the PDF associated with a given amount of subgrid-scale variability is more skewed at altitude than at low levels. It tends toward a Gaussian distribution (i.e., $k \to 0$) as $\sigma/(\mu - X) \to 0$.

The first statistical moment of the total water distribution (μ) is explicitely calculated by the prognostic equations of the model. We make the hypothesis that the second and third statistical moments can be diagnosed (i) from the in-cloud water content predicted by the convection scheme as a result of the convective activity that takes place within the domain, (ii) from the degree of saturation of the large-scale environment, and (iii) by insisting that the total water mixing ratio values are positive: we take $X = 0$.

c. Cloud amount and in-cloud water content

Using the above expressions, (5) and (6) with $X = 0$, we obtain

$$f = \frac{1}{2}\left[1 - \text{erf}\left(\frac{\delta}{k\sqrt{2}} - \frac{k}{2\sqrt{2}}\right)\right], \quad \text{and} \tag{12}$$

$$q_c^{\text{in}} = \mu\left[\frac{1 - \text{erf}\left(\dfrac{\delta}{k\sqrt{2}} + \dfrac{k}{2\sqrt{2}}\right)}{1 - \text{erf}\left(\dfrac{\delta}{k\sqrt{2}} - \dfrac{k}{2\sqrt{2}}\right)} - e^{-\delta}\right], \tag{13}$$

where δ is defined by $q_s = \mu e^{-\delta}$ (i.e., it is the logarithm of the domain-averaged relative humidity).

As $k \to 0$, $P(q_t)$ becomes equivalent to a Gaussian PDF (with $\lambda = \mu$ and $\alpha = \sigma$), and as $\sigma \to 0$ (which is a particular case of $k \to 0$), the Gaussian expression of the cloud fraction behaves as a Heaviside unit step function (Cotton and Anthes 1989). Therefore, in the limit $\sigma \to 0$, the generalized lognormal PDF becomes equivalent to an ''all-or-nothing'' large-scale saturation scheme that predicts the cloud fraction and the in-cloud water content as

$$\begin{cases} f^{\text{LS}} = 0 \text{ and } q_c^{\text{in,LS}} = 0, & \text{if } \mu \le q_s; \\ f^{\text{LS}} = 1 \text{ and } q_c^{\text{in,LS}} = \mu - q_s, & \text{if } \mu \ge q_s. \end{cases} \tag{14}$$

d. Determination of the second and third moments of the PDF

To ensure some continuity between the condensate produced at the subgrid scale and that produced at the large scale, we define the actual contribution of subgrid-scale processes to the total in-cloud water content as

$$q_c^{\text{in,SUB}} = q_c^{\text{in}} - q_c^{\text{in,LS}}, \tag{15}$$

where $q_c^{\text{in,LS}}$ is the contribution of large-scale processes given by (14), and q_c^{in} is the total in-cloud water content defined by (7) as a function of the large-scale variables $\overline{q_t}$ and $\overline{q_s}$, and of the parameter k. If $q_c^{\text{in,SUB}}$ is predicted within the parameterization of the subgrid-scale con-

[3] Note that for a similar reason, the fact that q_t is physically bounded from above may explain a slightly negative skewness at low atmospheric levels.

densation process (e.g., the convection scheme), then it is possible to predict the value of k that solves the system of equations composed by (13), (14), and (15). We use the iterative method of Newton for this purpose (appendix B). Parameter k is then a function of $q_c^{\text{in,SUB}}$, $\overline{q_t}$, $\overline{q_s}$, and X. From k, X, and μ, the variance and the skewness coefficient of the total water distribution can be inferred (appendix A).

In this study, we focus on the cloudiness associated with cumulus convection. However, the above framework may be extended to include the cloudiness associated with several subgrid-scale condensation processes (e.g., convective clouds, stratus, stratocumulus) by defining $q_c^{\text{in,SUB}}$ as the sum of several contributions, and then using (15) and (13) to predict the variance associated with the cumulative effect of the different processes, or by predicting a PDF for each condensation process and making a convolution between them.

e. Subgrid-scale in-cloud water content

In this study, the cloud water content is produced at the subgrid scale by cumulus convection and at the large scale by supersaturation. The condensate produced by cumulus convection is computed within the convective parameterization. In the Emanuel convection scheme, air is assumed to be lifted adiabatically from the subcloud layer to each level i between cloud base and cloud top. A fraction ϵ^i of the condensed water amount (CLW^i) produced during this ascent is converted to precipitation, and the remaining cloudy air [$\text{CLW}^i (1 - \epsilon^i)$] is mixed with the environmental air, forming a spectrum of mixtures that ascend or descend to detrain to the environment at their level j of neutral buoyancy. If the mixture ascends, additional condensation is produced (l^{ij}). It is then assumed that if the condensate mixing ratio in the mixture exceeds that of the undilute updraft after precipitation [i.e., if $l^{ij} > \text{CLW}^j(1 - \epsilon^j)$], the excess condensed water is converted to precipitation. The condensate mixing ratio produced by cumulus convection at the subgrid scale that we use in the cloud scheme ($q_c^{\text{in,SUB}}$) is computed as a linear combination of the condensed water in the undilute updraft and in the mixed drafts:

$$q_c^{\text{in,SUB}} = \sigma_a^i Q_a^i + (1 - \sigma_a^i) Q_m^i, \tag{16}$$

where σ_a^i is an estimate of the fractional area covered by the undilute updraft at level i, Q_a^i is the condensed water in the undilute updraft after precipitation [$Q_a^i = \text{CLW}^i(1 - \epsilon^i)$], and Q_m^i is the arithmetic mean of the condensed water mixing ratio of mixtures (saturated updrafts and downdrafts) after precipitation. When no air can entrain at level i, we take $Q_m^i = Q_a^i$ so that $Q^i = Q_a^i$. The fraction σ_a^i is estimated as $\sigma_a^i = M_a^i/\rho^i\omega_a^i$ with $\omega_a^i = \beta(2\text{CAPE})^{1/2}$ (M_a^i is the mass flux of the undilute updraft and ω_a^i its vertical velocity), with $\sigma_a^i > 1$. Here, β is a coefficient that should be smaller than 1 because $(2\text{CAPE})^{1/2}$ is an upper bound of the vertical velocity of the adiabatic updraft. Although this coefficient should in principle depend on the vertical profile of entrainment, in this study we set it equal to a constant value of 0.01. Note that σ_a^i being always small, $q_c^{\text{in,SUB},i} \simeq Q_m^i$. Indeed, clouds associated with cumulus convection are mainly composed of entrained air.

f. Illustration

Figure 1 illustrates how the predicted cloud fraction varies with the saturation excess (or deficit) of the environment and with the in-cloud water content produced by subgrid-scale processes. If $q_c^{\text{in,SUB}} = 0$, then the scheme is equivalent to an all-or-nothing cloud scheme: it predicts a zero cloud fraction if the environment is undersaturated, and overcast conditions if the environment is supersaturated. In the presence of subgrid-scale condensation, a fractional cloud amount is predicted, that increases with the degree of saturation (or relative humidity) or the environment. The impact on the cloud fraction of the positive skewness (seen by comparing the curves corresponding to low and high values of q_s, which are representative of lower and upper tropospheric levels, respectively) depends on the degree of saturation of the environment. It is generally stronger in subsaturated environments than in supersaturated environments.

3. Results using a single-column model

a. Main features of the model

To evaluate the coupled cloud-convection parameterization, we use the single column model developed by Emanuel and Zivkovic-Rothman (1999, hereafter referred to as EZ99). This model is used with a 25-hPa vertical resolution (40 vertical levels) to represent adequately the sharp vertical gradients of water vapor. The timestep is 5 min, although it can be substantially increased without modifying too much the performance of the model. This model is forced by observed large-scale advections of heat and moisture. To ensure the conservation of the integrated enthalpy during the experiment, observed, large-scale vertical velocities are corrected as explained in EZ99. Surface sensible and latent heat fluxes are computed interactively by using a deep convective downdraft velocity scale in the surface flux formulations, together with the observed surface wind speed.

We use version (4.3b) of the convection scheme, which has been optimized in its water vapor prediction using TOGA COARE data. Nevertheless, subsequent optimizations of the scheme (but prior to the use of the cloud and radiation schemes) lead us to use some parameter values different from those of EZ99 (Table 1). We introduce, in particular, a maximum precipitation efficiency $\epsilon_{\max}$ such that

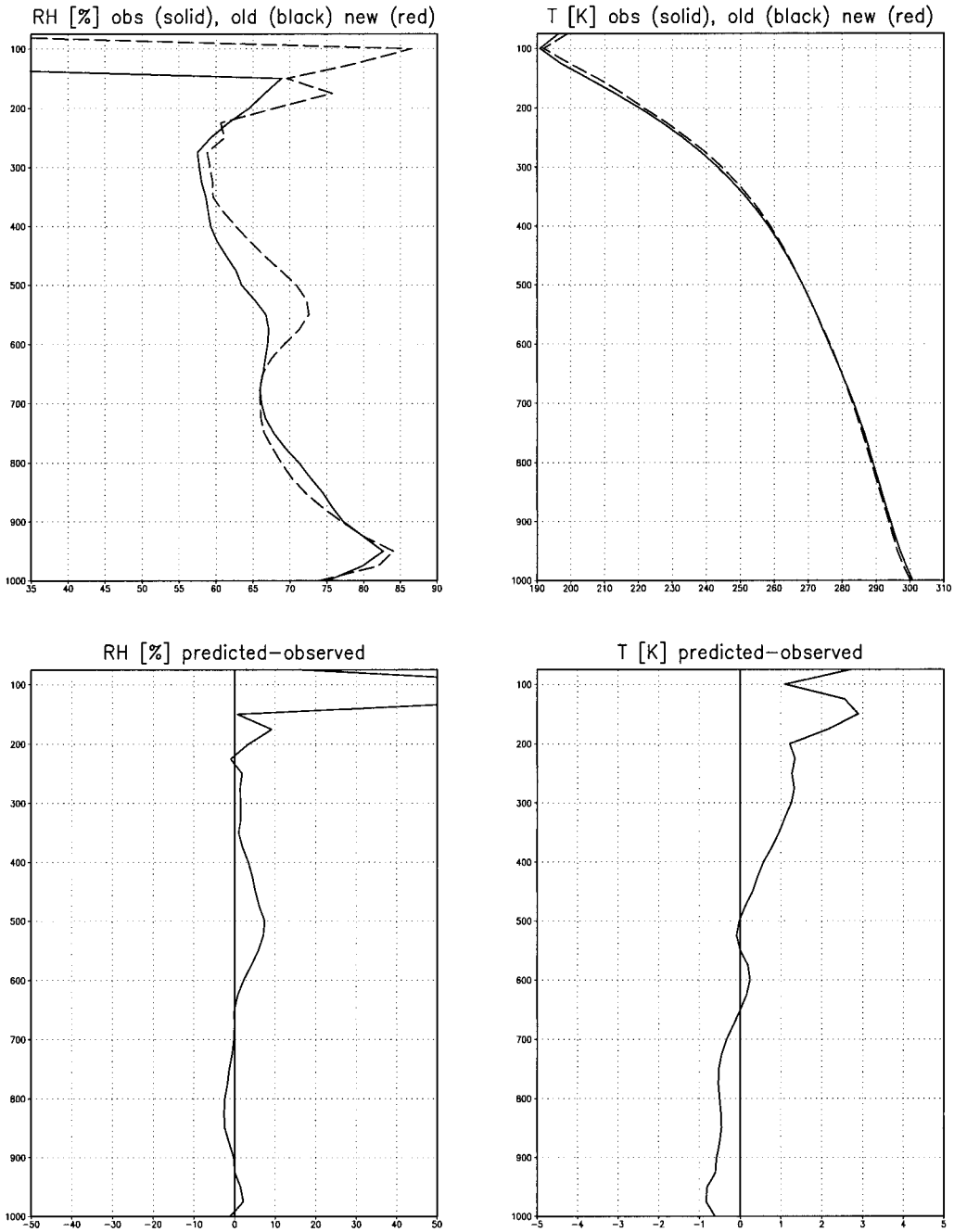

FIG. 2. Difference between predicted and observed relative humidity and temperature profiles averaged over the last 100 days of operation of the TOGA COARE IOP. Note that relative humidity measurements are not reliable above 300 hPa.

$$\epsilon_i = \left[1 - \frac{l_c(T^i)}{\mathrm{CLW}^i}\right]\epsilon_{\max}, \tag{17}$$

where ϵ_i, T^i, CLW^i, and $l_c(T^i)$ are the precipitation efficiency at level i, the in-cloud temperature, the in-cloud condensed water mixing ratio, and the temperature-dependent threshold condensed water value above which precipitation occurs, respectively. EZ99 set $\epsilon_{\max}$ to unity. Setting $\epsilon_{\max}$ to a value slightly less than unity (0.999) allows some cloud water to remain in suspension in the upper troposphere instead of being entirely rained out.

The single-column model (SCM) used by EZ99 included a large-scale supersaturation adjustment scheme that precipitated instantaneously all the water content exceeding saturation ($\overline{q_t} - q_s$). Thus, no cloud water was allowed to reside in the atmosphere. In the present

TABLE 2. Value of the different parameters used in the simple representation of cloud optical properties (CTRL experiment). Parameter ρ_l is the density of liquid water, P the pressure, and g is the gravity.

Parameter	Description	Value or definition
τ_{liq}	Optical thickness of liquid clouds	$\tau_{\text{liq}} = \frac{3}{2}\frac{q_{\text{liq}}^{\text{in}}\frac{\Delta P}{g}}{\rho_l r_{\text{liq}}}$
τ_{ice}	Optical thickness of ice clouds	$\tau_{\text{ice}} = \frac{3}{2}\frac{q_{\text{ice}}^{\text{in}}\frac{\Delta P}{g}}{\rho_l r_{\text{ice}}}$
r_{liq}	Effective radius of liquid particles	10 μm
r_{ice}	Effective radius of ice particles	30 μm
k_{liq}	Mass absorption coefficient for liquid water clouds	0.0783 m^2 g^{-1}
k_{ice}	Mass absorption coefficient for ice clouds	0.0542 m^2 g^{-1}
T_{liq}, T_{ice}	Transition temperatures used to compute the ice/liquid ratio a_{ice}	0, -15°C

version of the SCM, we compute a ''large-scale precipitation efficiency'' based on Eq. (17), T^i being in that case the domain-averaged temperature, and CLW^i the amount of cloud water exceeding saturation ($\overline{q_t} - q_s$). Although the parameter values entering (17) may be different for convective clouds and large-scale nonconvective clouds, we take them to be the same in this study, for the sake of simplicity.

b. Cloud optical properties

Here, rather than using observed top of atmosphere and surface radiative fluxes, as in EZ99, the radiative cooling is computed interactively by a radiation scheme using the shortwave parameterization of Fouquart and Bonnel (1980) and the longwave parameterization of Morcrette (1991). Radiative fluxes are computed at each vertical level every 3 h using instantaneous profiles of temperature, humidity, cloud fraction and cloud water path, and a climatological distribution of ozone. For these calculations, we assume that the vertical overlap of adjacent cloud layers is maximum while that of nonadjacent cloud layers is random.

The representation of cloud–radiation interactions requires some information about the cloud water phase and cloud optical properties. As the ice phase is not explicitely expressed in the convection scheme, we have to partition the cloud condensate into liquid and frozen cloud water mixing ratios. For this purpose, we define a cloud ice fraction a_{ice} set to unity for temperatures lower than a threshold temperature T_{ice}, zero for temperatures above T_{liq}, and varying linearily with temperature at intermediate temperatures (Table 2). The in-cloud liquid and frozen water mixing ratios are then defined as: $q_{\text{liq}}^{\text{in}} = q_c^{\text{in}}\,(1 - a_{\text{ice}})$ and $q_{\text{ice}}^{\text{in}} = q_c^{\text{in}}\,a_{\text{ice}}$.

The interaction of clouds with shortwave radiation is taken into account by computing, at each vertical level of the atmosphere, the cloud optical thickness as $\tau = \tau_{\text{liq}} + \tau_{\text{ice}}$ where τ_{liq} and τ_{ice} are the optical thicknesses of the liquid and frozen parts of clouds, respectively. The interaction of clouds with infrared radiation is represented by a cloud infrared emissivity defined by $\epsilon^{\text{IR}} = 1 - \exp(-D\,k_{\text{abs}} q_c^{\text{in}}\,\Delta P/g)$, where D is a diffusivity factor equal to 1.66, and k_{abs} an infrared mass absorption coefficient. When liquid and frozen parts coexist within a cloud, we compute it as $k_{\text{abs}} = (1 - a_{\text{ice}})\,k_{\text{liq}} + a_{\text{ice}}\,k_{\text{ice}}$ where k_{liq} and k_{ice} are mass absorption coefficients for the liquid and frozen parts, respectively.

Single-column model simulations are performed first by using a very simple representation of ice clouds' optical properties that assumes, in particular, a uniform specified effective radius for ice crystals. Observations indicate however that the effective size of ice crystals is actually highly variable and may vary from 20 to more than 80 μm in tropical cirrus anvils (Heymsfield and McFarquhar 1995). A second representation of ice clouds optical properties (referred to as ''ICE-OPT'') attempts to account for some in situ measurements of cirrus microphysical properties. In particular, it allows the effective radius of ice particules to vary with temperature, makes the mass absorption coefficient of ice clouds depend on the size of ice crystals, and uses a cloud optical thickness formulation that is presumably more suitable for ice clouds. A third experiment (referred to as ''PHASE'') is identical to ICE-OPT except that the definition of the frozen fraction of cloud water a_{ice} is modified. This is done by assuming that ice particules start forming at temperatures below -10°C (instead of 0°C), and that there are no more liquid particules at temperatures below -30°C. This modification is motivated by the observation that in convective clouds, liquid particles are found over a very wide range of temperatures (Bower et al. 1996). The three representations of cloud optical properties used in this study are summarized in Table 3.

c. Comparison of observed and predicted thermodynamic fields

As stressed by Emanuel (1991), relative humidity is likely to be the most sensitive predictand of moist pro-

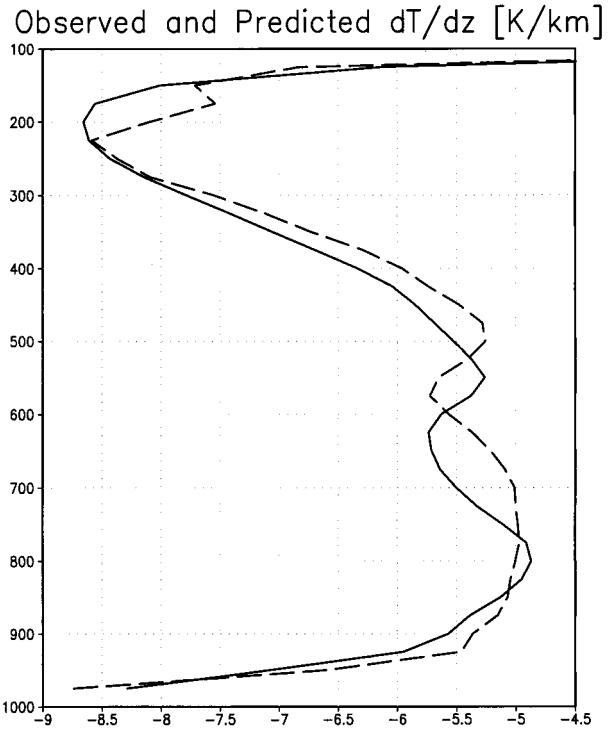

FIG. 3. Mean vertical profile of the temperature lapse rate observed from radiosondes (solid line) and predicted by the model (dashed line) during the TOGA COARE IOP.

cesses parameterizations. The performance of the coupled cloud-convection scheme is thus primarily based on comparison of the observed and predicted evolutions of relative humidity (RH) during the TOGA COARE experiment. Owing to the global enthalphy constraint, a good prediction of the humidity profile almost guarantees a good prediction of the temperature profile (EZ99). The mean RH and temperature profiles predicted by the SCM including the cloud and radiation schemes and observed by radiosondes during the last 100 days of operation of the TOGA COARE intensive flux array (IFA) are shown in Fig. 2. On average, the temperature bias in less than 1.2° up to 200 hPa, and the RH bias is less than 8%. These values are close to measurement uncertainties. The rms error, however, is larger. Vertically averaged between the surface and 300 hPa, the rms error of RH is 14.13% and that of temperature is 1.99 K. This is slightly less than with the version of the model without any cloud and radiation schemes (EZ99), although the model has not been reoptimized.

By promoting cloud detrainment at prefered atmospheric levels, stable atmospheric layers are expected to play a role in the vertical distribution of cloud tops, and thus in the relative population of the different cloud types over the IFA region (Zuidema 1998; Johnson et al. 1999). The prediction by a model of the temperature lapse rate is thus a potentially important influencing factor in the prediction of clouds. Figure 3 shows that the SCM including the convective, cloud, and radiation schemes reproduces the three main stable layers that have been suggested by the observations: at low levels (around 2 km), at the tropopause, and around 5 km near the freezing level. However, compared to observations, the simulated low-level inversion is less sharp, and the stable layer of the middle troposphere occurs about 1 km too high.

d. Predicted cloud fields

The mean fractional cloud amount and in-cloud water content predicted by the SCM during the last 100 days of operation of TOGA COARE are displayed in Fig. 4. On average, cumulus convection is responsible for at least 70% of the production of cloud condensate. This contribution even reaches 100% between the condensation level (around 925 hPa) and around 600 hPa. Indeed, as this portion of the atmosphere is subsaturated at the large-scale most of the time, the presence of cloud water is primarily due to the presence of subgrid-scale saturated updrafts and downdrafts that accompany shal-

TABLE 3. Summary of the representation of the cloud optical properties of ice clouds in the control experiment, and in the sensitivity experiments ICE-OPT and PHASE.

	CTRL	ICE-OPT	PHASE
r_{ice} (μm)	30	$0.71Tc + 61.29$[a] $r_{ice} = 3.5$ μm for $Tc < -81.4$°C[b]	$0.71Tc + 61.29$ $r_{ice} = 3.5$ μm for $Tc < -81.4$°C
τ_{ice}	$\frac{3}{2}\frac{q_{ice}^{in}\Delta P/g}{r_{ice}}$	$q_{ice}^{in}\frac{\Delta P}{g}\left(3.448 \times 10^{-3} + \frac{2.431}{r_{ice}}\right)$[c]	$q_{ice}^{in}\frac{\Delta P}{g}\left(3.448 \times 10^{-3} + \frac{2.431}{r_{ice}}\right)$
k_{ice} (m^2 g^{-1})	0.0542	$0.005 + \frac{1}{r_{ice}}$[d]	$0.005 + \frac{1}{r_{ice}}$
T_{liq}, T_{ice} (°C)	0, −15	0, −15	−10, −30

[a] Formula used by Suzuki et al. (1993), after the observational data of Heymsfield and Platt (1984); Tc is the temperature in Celsius.
[b] From Heymsfield (1986).
[c] From Ebert and Curry (1992). Here, $q_{ice}^{in}\Delta P g^{-1}$ is the in-cloud ice water path in g m^{-2} when r_{ice} is in μm.
[d] From Kiehl and Zender (1995), after Ebert and Curry (1992).

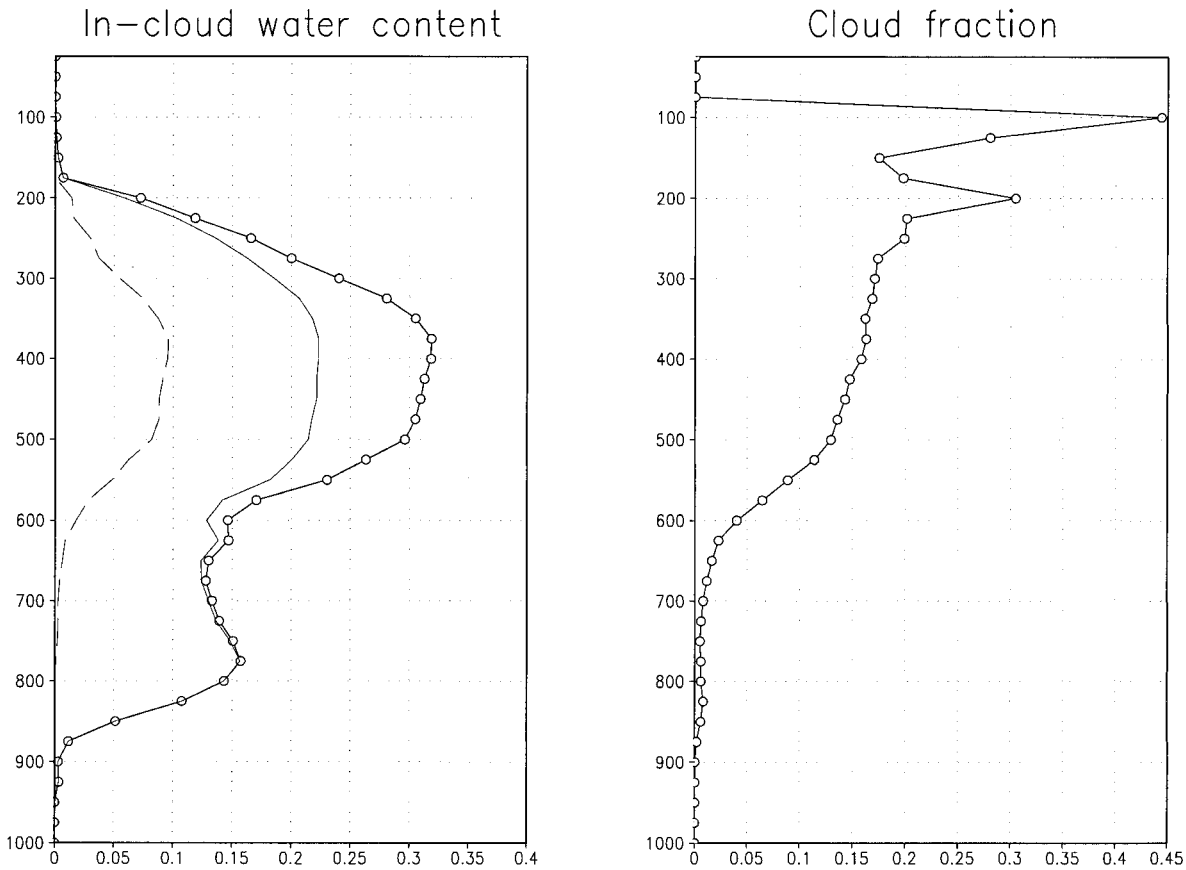

FIG. 4. In-cloud water content (in g kg^{-1}) predicted by the single-column model over the TOGA COARE IFA and averaged over the last 100 days of the IOP. The thin line represents the in-cloud water content produced at the subgrid-scale by cumulus convection and the dashed line that produced at the large-scale. The line with markers corresponds to the total (subgrid-scale + large-scale) in-cloud water content that actually interacts with radiation. (right) Cloud fraction predicted by the SCM and averaged over the same period.

low and deep convection. However, the associated cloud fraction is very small, owing to the large saturation deficit of the environment (Fig. 1). The cloud fraction increases significantly with height above the 600 hPa level (4–5 km). This is due to (i) the large amount of condensate produced by cumulus convection and, to a lesser extent, by large-scale condensation; and (ii) to the smaller saturation deficit of the environment. Maxima are found around 200 hPa (12–13 km), where the convective detrainment is maximum and significantly moistens the environment (not shown), and around 100 hPa (16.5 km), just below the tropopause, where the relative humidity is high. This average vertical distribution of the cloud cover results from the presence of different cloud types within the domain. This is discussed in the following section.

4. Evaluation

a. Prediction of radiative fluxes

Within the framework of the International Satellite Cloud Climatology Project (ISCCP), broadband radia-

TABLE 4. Comparison of observed and computed radiative fluxes at the top of the atmosphere and at the surface over the TOGA COARE IFA. Column headings represent: OLR (OLR_{clear}), the mean (clear sky) outgoing longwave radiation (W m^{-2}); α the planetary albedo (%); ASR_{clear}, the clear-sky absorbed shortwave radiation, (W m^{-2}); LW_{sfc} and SW_{sfc}, the surface net longwave and shortwave radiative fluxes (W m^{-2}) (derived from IMET data). Also reported are the root-mean-square errors against observations of the predicted OLR and planetary albedo.

	OLR	α	OLR_{clear}	ASR_{clear}	LW_{sfc}	SW_{sfc}	rms_{OLR}	rms_{α}
Observations	218	33.3	273	389	−58	187	0	0
CTRL	225	29.6	287	394	−65	214	39	16
ICE-OPT	220	32.0	286	394	−64	204	37	16
PHASE	223	33.0	286	394	−64	199	38	16

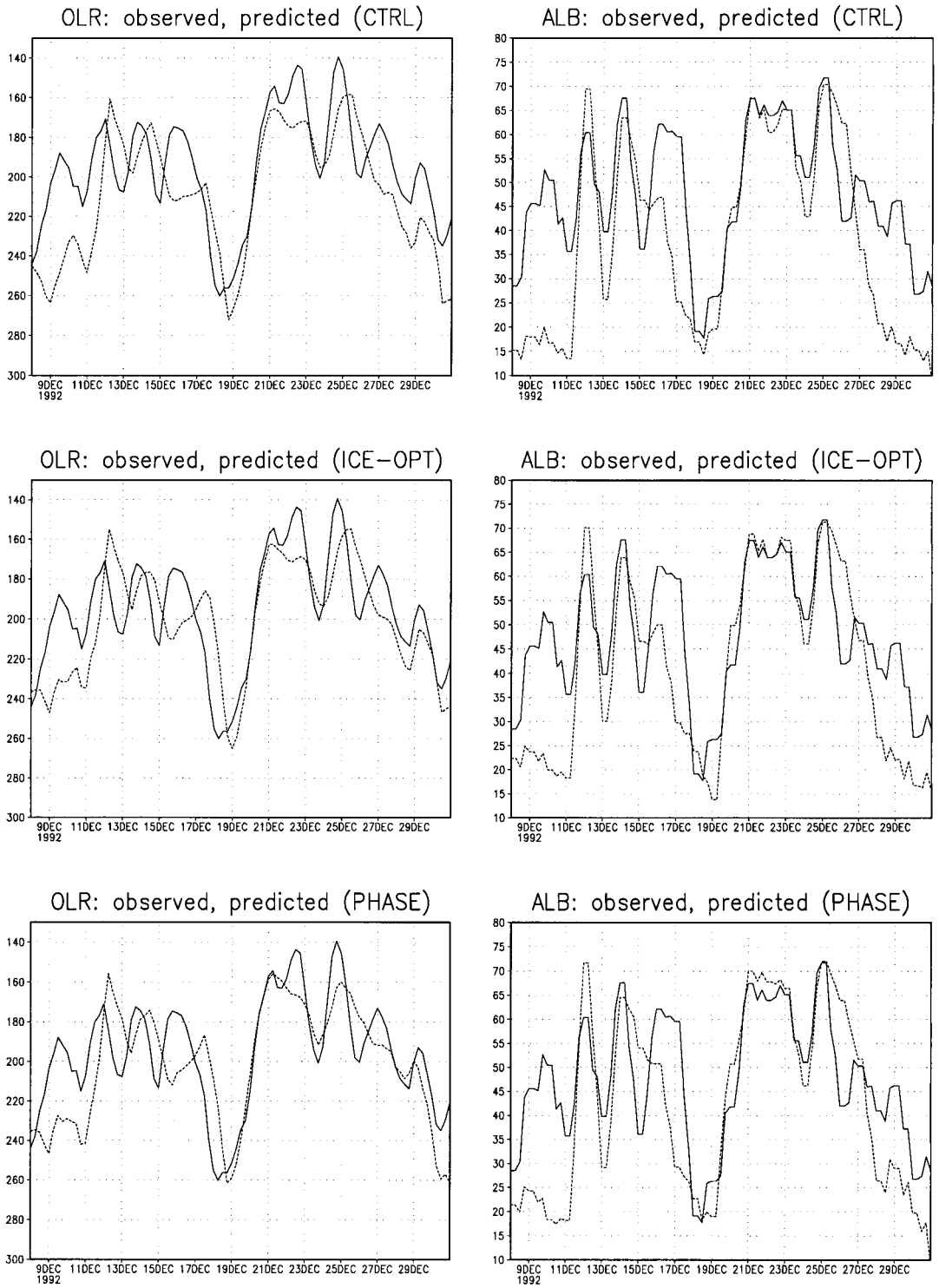

FIG. 5. Comparison of the observed (solid line) outgoing longwave radiation (OLR, W m^{-2}) and planetary albedo (%) at the top of the atmosphere with that predicted (dashed line) by the single-column model using different representations of cloud optical properties: a very simple one [control (CTRL) experiment] or a more sophisticated representation of ice optical properties (ICE-OPT). The PHASE experiment uses the same cloud optical properties than the ICE-OPT experiment, but the definition of the liquid/frozen ratio of cloud water is modified (1-day running means).

TABLE 5. Comparison of SST, top-of-atmosphere and surface radiation and surface latent and sensible heat fluxes (LH, SH) observed and computed by the single-column model in simulations with interactive (predicted) SST. Model results are reported for three simulations using different representations of the cloud optical properties. The $CTRL_{SST}$, $ICE\text{-}OPT_{SST}$, and $PHASE_{SST}$ experiments are identical to the CTRL, ICE-OPT, and PHASE experiments except that the SST is predicted, instead of specified from observations. Surface data are derived from IMET buoys. All variables are averaged over the last 100 days of the TOGA COARE IOP.

		Observations	$CTRL_{SST}$	$ICE\text{-}OPT_{SST}$	$PHASE_{SST}$
SST	C	29.3	30.1	29.7	29.6
OLR_{toa}	W m^{-2}	218	231	224	224
$albedo_{toa}$	%	33.3	26.8	30.6	31.8
LW_{sfc}	W m^{-2}	−58	−67	−65	−65
SW_{sfc}	W m^{-2}	187	227	211	205
LH_{sfc}	W m^{-2}	106	145	137	134
SH_{sfc}	W m^{-2}	8	12	11	11

tive fluxes at the top of the atmosphere over the TOGA COARE IFA were derived from radiances measured on board the geostationary meteorological satellite (the so-called ''FC dataset''; Zhang et al. 1999). We use these data to evaluate the outgoing longwave radiation (OLR) and the planetary albedo calculated on line from the predicted profiles of temperature, humidity, cloud fraction, and cloud water content by using three different representations of the optical properties of ice clouds. (section 3a).

Table 4 shows that on average, the clear-sky OLR and absorbed shortwave radiation are 14 and 5 W m^{-2} larger than ISCCP estimates, respectively. Since the model is forced by observed SSTs and is optimized in its RH prediction (Fig. 2), it seems unlikely that biases in the prediction of humidity and temperature profiles are fully responsible for such a difference between observed and calculated fluxes. Iacobellis and Somerville (2000) suggested that ISCCP clear-sky fluxes at the top of the atmosphere may be biased by approximately the same order of magnitude. Their interpretation, supported by radiative calculations, is that subvisible cirrus clouds located near the tropical tropopause are too thin to be detected by ISCCP, but may decrease the (oth-

TABLE 6. Summary of the different cloud parameterizations considered in this study [note that the scheme referred to as Smith (1990) is actually a slightly simplified version of the original Smith's scheme]. The type of PDF considered and the definitions of the variance and of the skewness coefficient for each scheme is reported.

Scheme	PDF	Variance	Skewness
This study	Generalized lognormal	$\sigma = \lvert\overline{q}_t - X\rvert\sqrt{e^{k^2} - 1}$	$S = \dfrac{(\overline{q}_t - X)^3}{\sigma^3}[2 - 3e^{k^2} + (e^{k^2})^3]$
			$X = 0$ (lower bound)
		k such that: $q_c^{in}(\overline{q}_t, \overline{q}_s, k, X) = q_c^{in,sub}* + q_c^{in,ls}**$	
	Gaussian	σ, σ such that:	$S = 0$
		$q_c^{in}(\overline{q}_t, \overline{q}_s, \sigma) = q_c^{in,sub} + q_c^{in,ls}$	
	Triangular	$\sigma = \dfrac{\delta}{\sqrt{6}}$, δ such that:	$S = 0$
		$q_c^{in}(\overline{q}_t, \overline{q}_s, \delta) = q_c^{in,sub} + q_c^{in,ls}$	
	Uniform	$\sigma = \dfrac{\delta}{\sqrt{3}}$, δ such that:	$S = 0$
		$q_c^{in}(\overline{q}_t, \overline{q}_s, \delta) = q_c^{in,sub} + q_c^{in,ls}$	
Smith (1990)	Triangular	$\sigma = \dfrac{\delta}{\sqrt{6}}$, $\delta = \overline{q}_s(1 - RH_{crit})$	$S = 0$
		RH_{crit} tunable constant	
LeTreut and Li (1991)	Uniform	$\sigma = \dfrac{\delta}{\sqrt{3}}$, $\delta = \gamma\overline{q}_t$	$S = 0$
		γ = tunable constant	

* $q_c^{in,sub}$ is predicted from the convection scheme.
** $q_c^{in,ls} = q_c^{in,ls}(\overline{q}_t, \overline{q}_s)$.

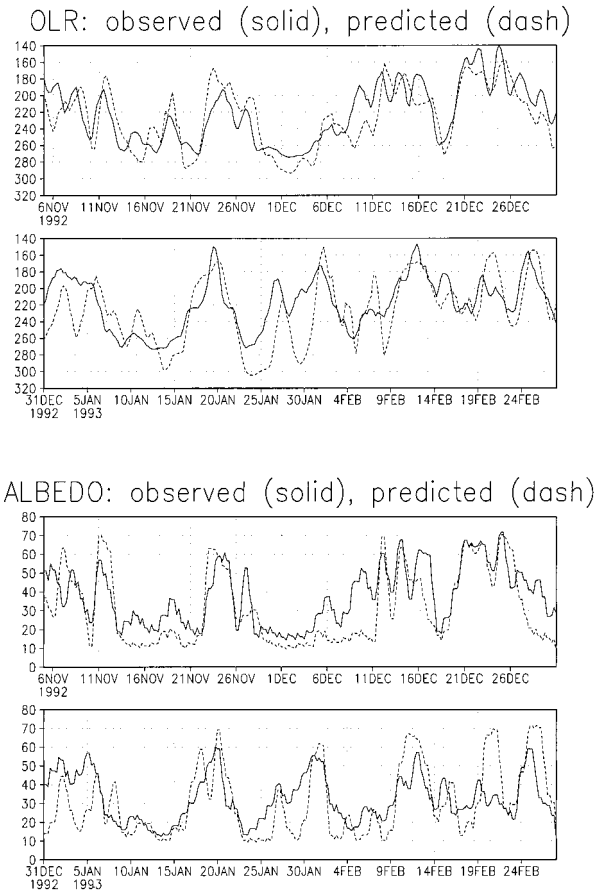

FIG. 6. Outgoing longwave radiation (OLR, in W m^{-2}, the vertical axis is flipped) and planetary albedo (%) derived from satellite measurements at the top of the atmosphere and predicted by the SCM (1-day running mean).

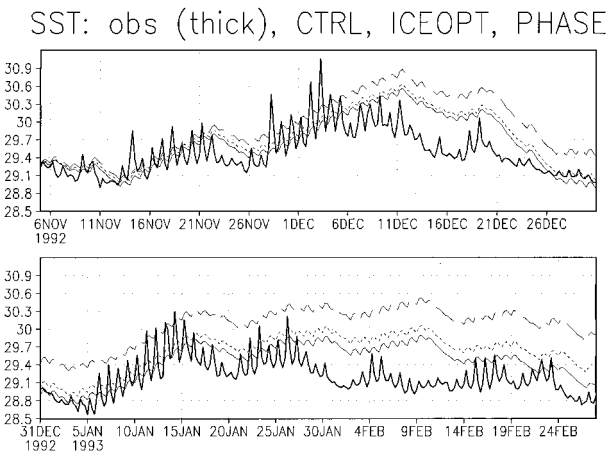

FIG. 7. Comparison of the observed (thick line) and predicted (thin lines) SSTs during TOGA COARE. Three model experiments are presented: $CTRL_{SST}$ (long-dashed line), which uses a very simple representation of cloud optical properties; $ICE\text{-}OPT_{SST}$ (dotted line), which uses a more sophisticated representation of ice optical properties; and $PHASE_{SST}$ (thin solid line), which uses the same cloud optical properties than $ICE\text{-}OPT_{SST}$ but uses a different definition of the liquid/frozen ratio of cloud water.

erwise clear-sky) OLR by 12 W m^{-2} and increase the reflected SW radiation by 4 W m^{-2}. Based on their radiative calculations, our model may therefore predict reasonable clear-sky radiative fluxes.

On average over the last 100 days of operation of TOGA COARE, the SCM overestimates the OLR by 2–7 W m^{-2} (the range indicates the sensitivity of the results to the type of representation of cloud optical properties), and underestimates the planetary albedo by 0%–4% (Table 4). Larger biases occur on a day-to-day basis, as shown by the larger magnitude of rms errors (Table 4). These errors may be due to errors in the simulation of the cloud field itself (cloud fraction and cloud water content), in the model-produced temperature and humidity profiles (the rms error or relative humidity and temperature are about 14% and 2 K, respectively), and presumably also in the forcing (in particular the absence of horizontal large-scale advections of hydrometeors, which are not available in the TOGA COARE dataset, plus the uncertainty associated with the empirical correction applied to ensure the conservation of the integrated enthalpy), as well as in the verification data. However, the fact that rms errors are quite similar among the three experiments shows that the fluctuations in time of the cloud cover and cloud water content are the primary modulators of the radiation fields, and that uncertainties in the representation of cloud optical properties (e.g., the effective radius of cloud particles) have in comparison a much smaller radiative impact. Consistently, the time-evolution of the radiative fluxes predicted in the three experiments during periods of intense convection (when the representation of ice cloud properties is likely to be the most critical) are very similar (Fig. 5).

Figure 6 shows that the OLR tends to be overestimated and the planetary albedo underestimated during episodes of suppressed convection. This suggests an underestimate of shallow-level clouds by the model. The inspection of observed and predicted relative humidity profiles reveals that the lower troposphere is systematically too dry during these situations (not shown). By underestimating the cloud fraction, this dryness certainly contributes to the observed biases in radiation. Another candidate to the lack of low-level cloudiness is the absence of negative skewness in the PDF of total water. At low levels, taking into account that the total atmospheric water is bounded by a maximum value may improve this situation. However, we have not found so far an upper bound that provides satisfying results and further work is necessary to find a suitable one. CRM simulations of these situations would certainly provide a helpful guidance for that purpose. During episodes of intense convection, the model discrepancies are not systematic and are therefore more difficult to interpret.

TABLE 7. Sensitivity of the bias and rms error of the predicted OLR and planetary albedo α to the choice of the PDF in the cloud parameterization proposed in this study. The CTRL, ICE-OPT, and PHASE experiments differ in their representation of the optical properties of ice clouds (see Table 3 for a description of these experiments).

	CTRL		ICE-OPT		PHASE	
PDF	(W m^{-2})	(%)	(W m^{-2})	(%)	(W m^{-2})	(%)
	Bias OLR	Bias α	Bias OLR	Bias α	Bias OLR	Bias α
Generalized lognormal	7	−4	2	−1	5	0
Gaussian	−5	−2	−6	1	−5	2
Triangular	−7	4	−9	6	−9	8
Uniform	−5	0	−6	3	−7	4
	rms OLR	rms α	rms OLR	rms α	rms OLR	rms α
Generalized lognormal	39	15	37	16	38	16
Gaussian	43	16	42	17	41	17
Triangular	39	15	41	16	40	17
Uniform	42	16	41	15	41	16

b. Prediction of sea surface temperatures

The time evolution of the warm pool SST results from a complex interplay of radiative, turbulent and oceanic processes. Surface data collected from improved meteorological instrumentation (IMET) buoys reveal that on average over the last 100 days of operation of TOGA COARE, the ocean gains 129 W m^{-2} by radiation and looses 114 W m^{-2} by latent and sensible heat fluxes (Table 5). The mean imbalance of 15 W m^{-2} over the IFA may result from measurement errors, but also from the loss of solar radiation through the bottom of the ocean mixed layer, and from ocean heat transports. TOGA COARE studies suggest that, in general, horizontal advection is not very important for setting SST in the warm pool region (Godfrey et al. 1998), except during episodes of westerly wind bursts where heat advection by ocean currents represents a significant contribution to the heat budget of the ocean mixed layer (Feng et al. 1998). On the other hand, Chou et al. (2000) suggest that the solar radiation penetrating through the bottom of the mixed layer is significant during the TOGA COARE intensive observation period (IOP). In any event, the data suggest that the radiative and turbulent fluxes at the ocean surface are the main contributors to the SST evolution on the timescale of 100 days. The comparison between the observed SST and that predicted by the model using calculated surface fluxes (shortwave and longwave radiation; latent and sensible heat) constitutes therefore an indirect assessment of the realism of the convection-cloud parameterization used in the model.

By neglecting horizontal advections and vertical entrainment of ocean water, and neglecting the penetration of solar radiation through the bottom of the mixed layer, we predict the SST evolution in the model by using the following equation:

$$C_l \rho_l H \frac{d\mathrm{SST}}{dt} = \mathrm{SW}_{\mathrm{sfc}} + \mathrm{LW}_{\mathrm{sfc}} - \mathrm{LH} - \mathrm{SH}, \quad (18)$$

where C_l, ρ_l, and H refer to the specific heat of liquid water, the density of liquid water and the depth of the ocean surface mixed layer. Parameters $\mathrm{SW}_{\mathrm{sfc}}$, $\mathrm{LW}_{\mathrm{sfc}}$, LH, and SW are the net shortwave and longwave radiative fluxes and the latent and sensible heat fluxes at the ocean

TABLE 8. Sensitivity of the bias and rms error of the predicted OLR and α to the way the variance of the total water PDF is predicted. The prediction of the variance as a function of the saturation humidity and of a specified critical relative humidity, $\mathrm{RH}_{\mathrm{crit}}$, is that proposed by Smith (1990); the prediction of the variance as a function of the mean total water and of a tunable coefficient, γ ($\gamma = 0.2$), is that proposed by Le Treut and Li (1991). The Dirac PDF corresponds to an all-or-nothing cloud scheme (no representation of the subgrid-scale cloudiness).

		CTRL		ICE-OPT		PHASE	
PDF	Statistical moments	rms OLR (W m^{-2})	rms α (%)	rms OLR (W m^{-2})	rms α (%)	rms OLR (W m^{-2})	rms α (%)
Triangular	$\sigma = \dfrac{\delta}{\sqrt{6}}$, $S = 0$,						
	where $\delta = \overline{q}_s(1 - \mathrm{RH}_{\mathrm{crit}})$,	51	18	49	19	48	19
	δ such that $q_c^{\mathrm{in}}(\overline{q}_t, \overline{q}_s, \delta) = q_c^{\mathrm{in,sub}} + q_c^{\mathrm{in,ls}}$	39	15	41	16	40	17
Uniform	$\sigma = \dfrac{\delta}{\sqrt{3}}$, $\delta = \gamma\overline{q}_t$, $S = 0$,						
	where $\delta = \gamma\overline{q}_t$,	49	19	48	19	49	19
	δ such that $q_c^{\mathrm{in}}(\overline{q}_t, \overline{q}_s, \delta) = q_c^{\mathrm{in,sub}} + q_c^{\mathrm{in,ls}}$	42	16	41	15	41	16
Dirac	$\sigma = 0$, $S = 0$	53	21	52	19	52	20

surface. Although the depth of the surface mixed layer undergoes considerable variations during the 4 months of TOGA COARE, we use for H a constant value of 14.8 m, which is close to the mean depth observed during the experiment (Anderson et al. 1996). The SST is initialized on 1 November 1992 from its observed value.

The comparison of the observed SST with that calculated by the model (Table 5) shows that the model predicts the 100-day averaged SST with a bias ranging from 0.3 to 0.8 K depending on the assumed optical properties of ice clouds. Despite a significant sensitivity to the representation of the cloud optical properties, the surface shortwave heating is systematically overestimated by the model, and the ocean cooling by longwave radiation and surface heat fluxes is also overestimated correspondingly. A representation of the penetration of solar radiation through the ocean mixed layer may correct part of this excess in cooling by surface fluxes.

Figure 7 shows that diurnal variations of the SST are strongly underestimated by the model. This feature, which appears also in some CRM simulations (Wu et al. 1998), is likely to be related in part to the fact that observed SSTs are skin temperatures and are thus very sensitive to diurnal variations of the insolation and to fresh water effects associated with precipitation. On the other hand, the model reproduces the long-term variations of the SST. During the westerly wind bursts starting on 11 December 1992, it predicts the increase of the surface heat fluxes and the decrease of the surface net radiation that are associated with episodes of strong atmospheric convection (not shown). Nevertheless, the model tends to overestimate the surface radiative heating during periods of suppressed convection, which leads to an overestimate of the SST. Improving the representation of shallow-level clouds during periods of suppressed convection should certainly lessen this excessive surface heating.

c. *Consistency with CRM results*

Xu and Randall (1996a,b) analyzed results produced by explicit simulations of observed tropical cloud systems during GATE to point out some of the main physical and statistical properties that cloud parameterizations should obey. We presume that the first-order results of these studies are not specific to the cloud systems of GATE but reveal instead the general behavior of an

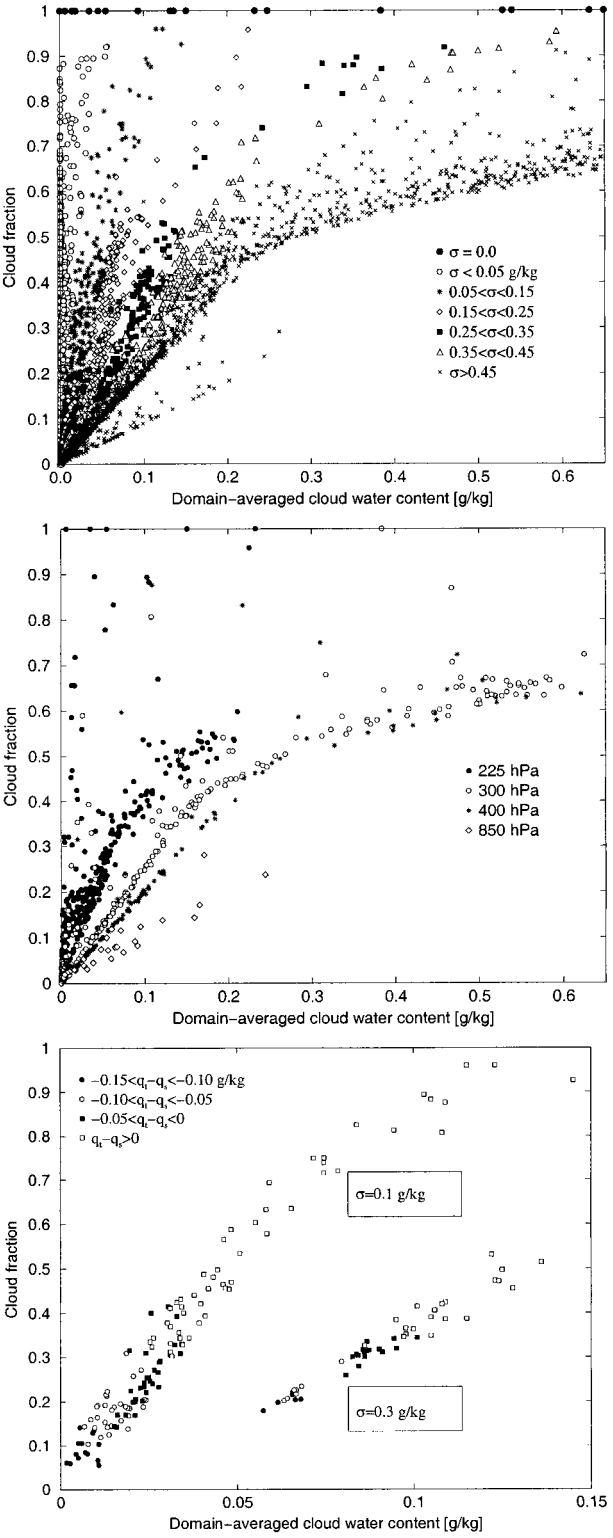

→

FIG. 8. Scatterplot diagram of the predicted cloud fraction vs the domain-averaged cloud water content for the last 100 days of the TOGA COARE IOP (a) stratified by the subgrid-scale variance of the total water content within the IFA domain (b) at different vertical levels of the atmosphere (c) stratified by the saturation deficit ($\overline{q_t} - \overline{q_s} < 0$) or excess ($\overline{q_t} - \overline{q_s} > 0$) of the environment [results are shown for two specified values of the subgrid-scale variance (σ) of the total water mixing ratio within the IFA domain].

ensemble of convective cloud systems over tropical oceans. The purpose of this section is to assess the ability of our cloud parameterization to reproduce these results when forced by TOGA COARE data. XR96b used some criteria based on the intensity of the simulated cloud drafts to divide the simulated cloud amount into ''convective'' and ''stratiform'' components, and presented results only for the stratiform component. However, the convective cloud amount found by XR96b is generally less than 6% at all levels; the domain-averaged stratiform cloud fraction and cloud water are presumably close to those that would be associated with the whole spectrum of clouds.

XR96a show that the domain-averaged relative humidity is not a good predictor of the stratiform cloudiness associated with deep convection. On the other hand, they show that the grid-averaged mixing ratio of condensate is a much better one, but that the predicted cloud fraction should also depend on the horizontal inhomogeneities of subgrid-scale circulations. In particular, they show that the cloud cover varies with the intensity of convective circulations (measured in their study by the cloud mass flux) in the stratiform regions. Our cloud parameterization is such that by construction, this effect is reproduced: for a given grid-averaged condensate content, in an environment supersaturated (subsaturated) the predicted cloud fraction decreases (increases) as the variance of the total water fluctuations increases within the domain (Fig. 8a). Moreover, as found in CRM simulations by XR96a, the slope of the relationship between the domain-averaged mixing ratio of condensate and the cloud fraction is steeper at upper levels than at low levels. This feature is also verified by our cloud parameterization (Fig. 8b), and simply reflects the increase of the precipitation efficiency with altitude. Finally, as suggested by XR96a, for a given amount of subgrid-scale heterogeneities, the cloud fraction increases as the degree of saturation of the environment (or RH) increases (Fig. 8c).

As explained in section 2b, the lognormal PDF of q_t is theoretically expected to be more skewed at altitude than at low levels. Figure 9 shows that this expectation is verified in actual SCM simulations of the TOGA COARE experiment. At low levels, the predicted PDF is very close to a normal distribution, while it is more and more skewed as the altitude increases. In this respect, the cloud parameterization presented in this study fulfils a strong requirement suggested by CRM simulations in stratiform regions of cumulus convection (XR96b).

d. Consistency with cloud observations

The cloud fraction and water content predicted by the model during the 120 days of operation of TOGA COARE undergo large temporal fluctuations, and cover a large range of values over a large range of vertical levels (Fig. 10). The simulation exhibits different cloud types that may be classified in four populations: low-level clouds associated with shallow convection, mid-level clouds, deep convective clouds with anvils, and thin cirrus clouds located just below the tropopause.

Some low-level clouds occur between 800 and 900 hPa (around 1.5–2 km). While these clouds are associated with significant concentrations of condensed water, their cloud fraction is small (less than 20%) due to the large saturation deficit of the low-level troposphere. Indeed, extensive stratiform low-level clouds were not commonly observed during TOGA COARE (D. Raymond 2000, personal communication), and low-level clouds were essentially of small cumulus type. A minimum cloud coverage occurs around 700 hPa (around 3 km), as is observed (Zuidema 1998). Nevertheless, clouds occur sometimes at this level (e.g., on 12 December 1992) when the temperature lapse rate becomes more unstable and the stable layer less pronounced below the 800-hPa level (not shown). This is consistent with the interpretation by Zuidema (1998) of the 700-hPa minimum in cloud cover.

The cloud fraction predicted by a single-column model at a particular vertical level should not be considered as the fractional area of a single cloud but that of a population of clouds present at this level. The simulation exhibits a large occurrence of clouds at middle-levels. These clouds occur either in association with upper level clouds or in isolation. Examples of this last category are predicted in November 1992, December 1992, and January 1993. As illustrated by Fig. 11, this population of clouds seems to be favored by the presence of a stable layer around the freezing level, as is suggested by the observations (Johnson et al. 1999).

A third population of clouds is characterized by vertically deep and horizontally extended cloud fractions (Fig. 10). These clouds occur particularly during 11–28 December 1992 and 9–28 February 1993, which correspond to convectively active periods of the intra-seasonal oscillation (Chen et al. 1996). The prediction of their occurrence coincides very closely with times for which the analysis of satellite data (Chen et al. 1996) reveals the presence of convective systems of class 3 and 4 (i.e., for which the square root of the cloud cluster's area ranges between 170 and 600 km). An interesting feature of these systems is the time evolution of their vertical structure (cloud fraction; water content). The cloud fraction associated with episodes of deep convection initially covers a large depth of the troposphere, typically from 500–600 hPa (4–5 km) up to 200 hPa (12–13 km), and then concentrates more and more at upper levels. Typical examples of this feature occur in December 1992 and February 1993 (Fig. 12). Since we predict the cloudiness that is associated with a spectrum of convective drafts, the evolution of the cloud cover is related to the evolution of the convective activity within the IFA domain. At the initial stage of the convective episode, a large amount of condensate is produced at the subgrid-scale and, to a lesser extent, at the large-scale. Due to the subgrid-scale variability, a small

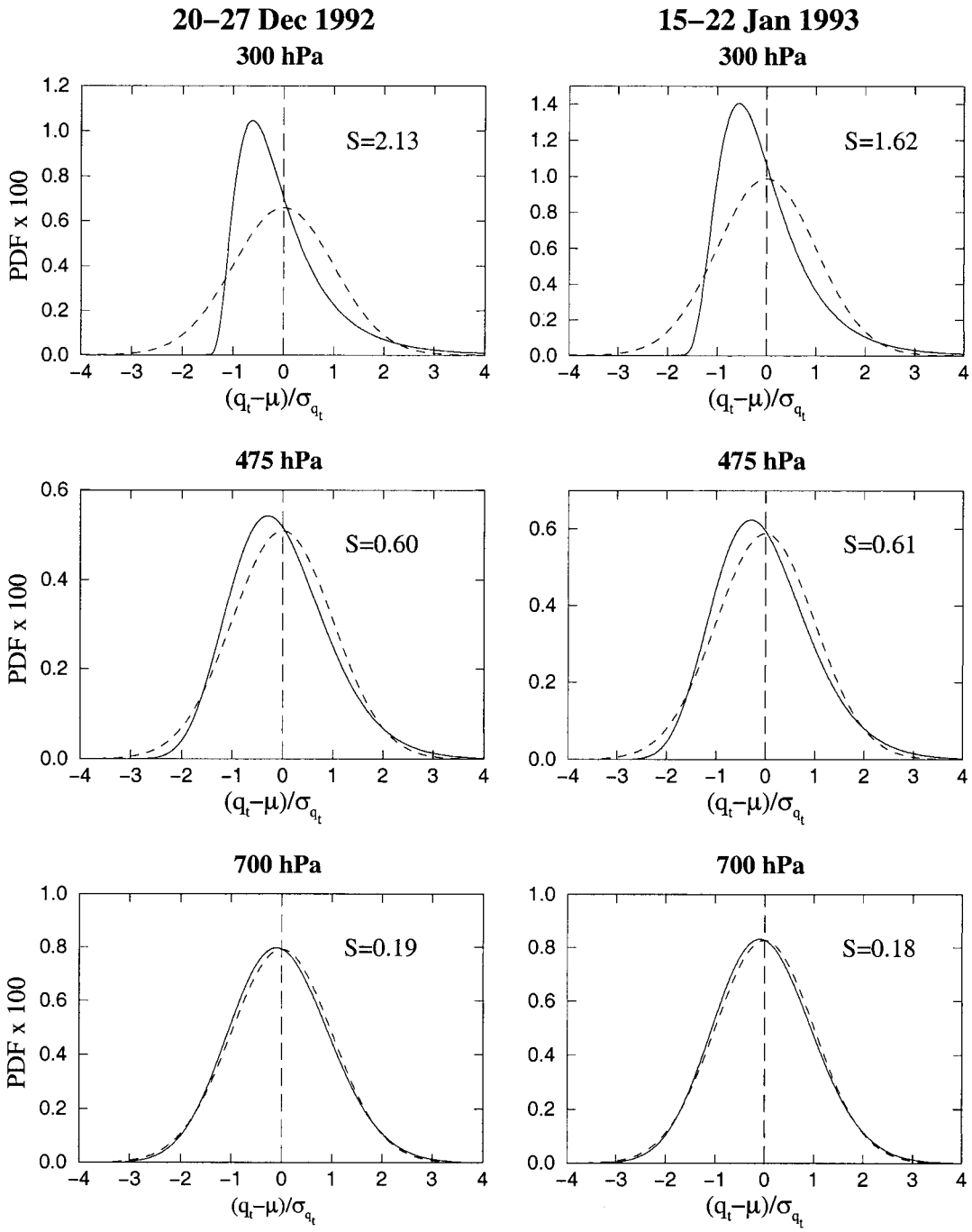

FIG. 9. PDFs plotted for different pressure levels using the location, scale and shape parameters derived from the TOGA COARE simulation and averaged over 20–27 Dec 1992 or 15–30 Jan 1993. The solid and dashed lines represent the generalized lognormal PDF (defined by parameters λ, α, and k) and Gaussian PDF (defined by parameters $\lambda = \mu$ and $\alpha = \sigma$), respectively. Variable S is the mean skewness coefficient.

cloud fraction can occur at low levels (at pressures higher than 600 hPa) despite a subsaturated environment. This is likely to represent the shallow and midlevel population of clouds observed over the IFA in the vicinity of cumulonimbus clouds (Johnson et al. 1999). As observed, this population tends to disappear as the SST decreases (not shown). The maturation of the convective cloud systems is associated with the development of convective downdrafts primarily driven by the evaporation of precipitation. These downdrafts occur over a larger and larger depth of the troposphere as the systems develop. The larger abundance of convective down-

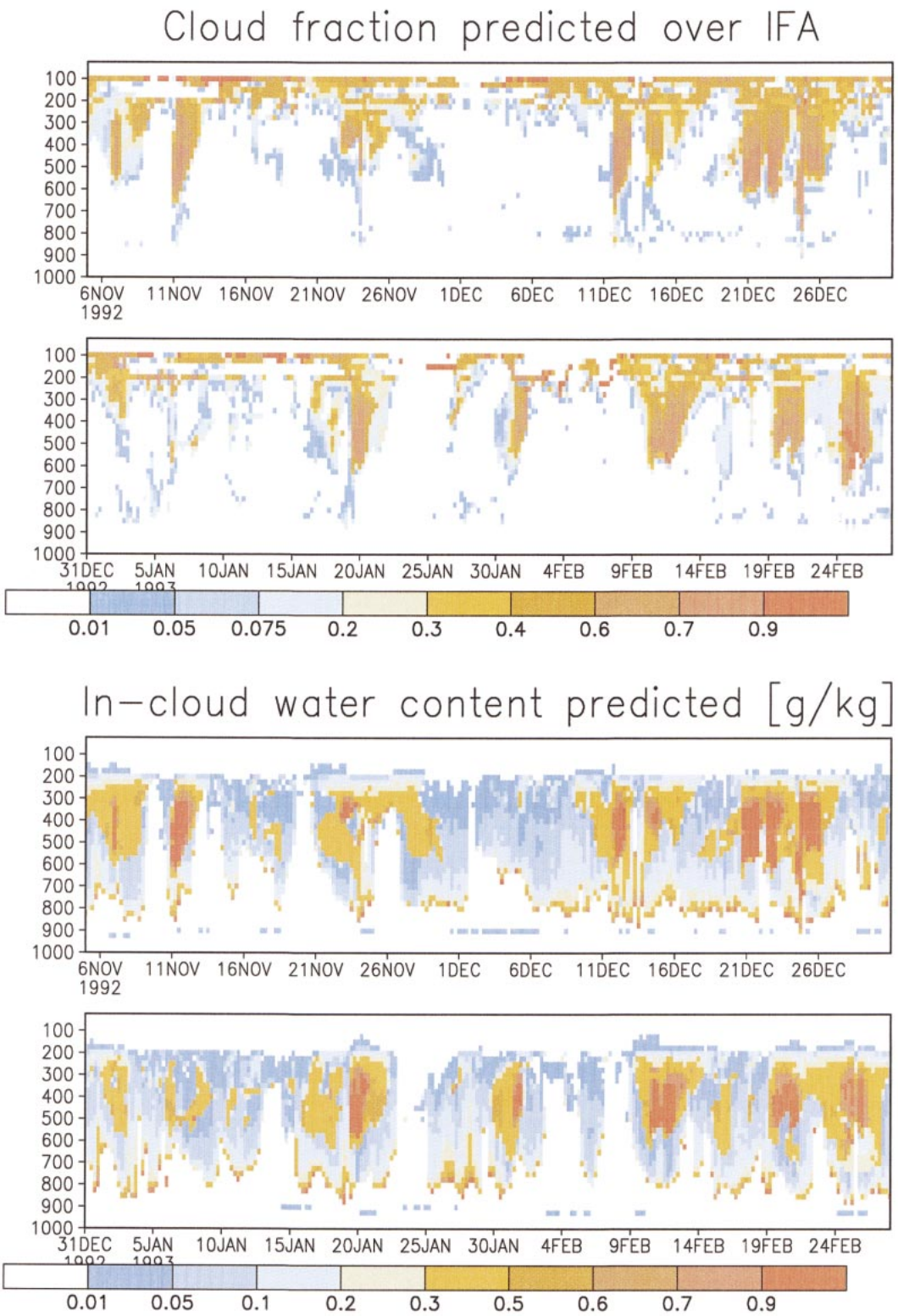

FIG. 10. (top) Time evolution of the fractional cloud amount and (bottom) of the in-cloud water content predicted by the model over the TOGA COARE IFA.

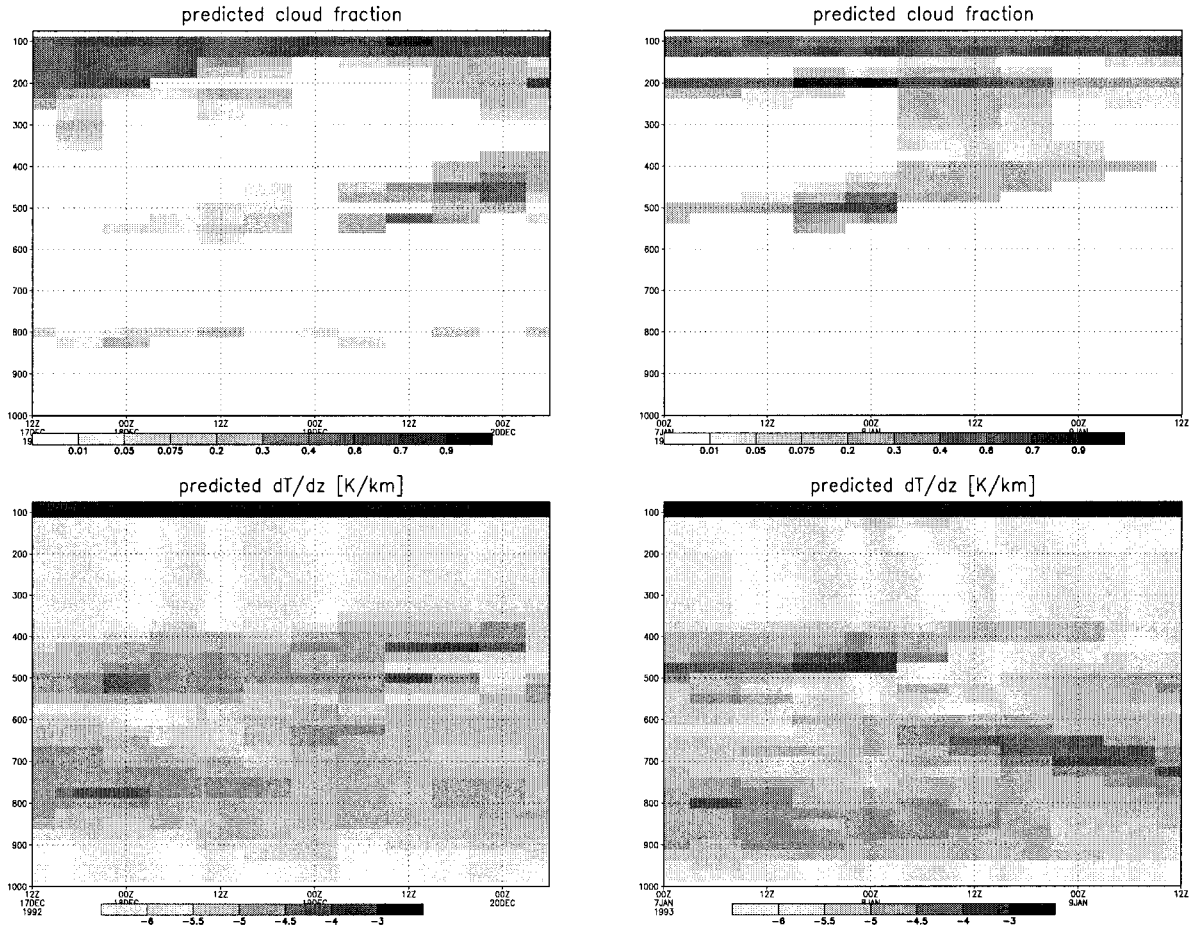

FIG. 11. Time evolution of the vertical profiles of cloud fraction and temperature lapse rate predicted by the model during 17–20 Dec 1992 and 7–9 Jan 1993.

drafts (and the smaller abundance of convective updrafts) inhibits the production of condensed water at the subgrid scale, and dries out the atmosphere by advecting some dry air downward. In subsaturated regions, a decrease of the subgrid-scale condensed water leads to a decrease of the cloud fraction (Fig. 1). Therefore, the collective effect of the maturation of cloud systems within the IFA leads to a progressive decrease of the cloud cover at lower and middle levels, while the cloud fraction (anvil) increases at upper levels. This is a commonly observed feature (e.g., Chen and Houze 1997). As shown in (section 4a), the occurrence of these thick anvil clouds is associated with planetary albedos exceeding 0.40, as observed by Heymsfield et al. (1998). Note that the evolution with time of the cloud cover primarily results from the evolution of the subgrid-scale convective activity that is internally predicted by the model, and its effect upon the large-scale saturation of the environment. The large-scale forcing, illustrated in Fig. 12 by the large-scale vertical velocity, seems to play a secondary role in this process.

Finally, a fourth population of clouds is predicted just below the tropopause (15–16 km, 100 hPa). This layer of ice clouds is usually separated from the top of anvil clouds by a few kilometers, except during the convectively active periods of the intraseasonal oscillation (11–28 December 1992, 9–28 February 1993) where anvil tops reach higher altitudes (Fig. 10). These clouds present some similarities with the cirrus detected near the tropical tropopause by satellite and lidar measurements (e.g., Wang et al. 1994; Jensen et al. 1996). As shown in Fig. 13, these clouds are associated with high relative humidities at the tropopause level (about 86% on the average). This is in agreement with satellite observations showing that the extreme tropical upper troposphere is often near saturation with respect to ice (Jensen et al. 1999). However, Fig. 13b indicates that the presence of clouds at the tropopause level would be much less frequent if it were related only to episodes of large-scale saturation. In our model, the cloud water content at 100 hPa is mostly produced by the convection. The effect of high relative humidities in the environment is to allow these tiny amounts of condensate (a few mg kg^{-1}, Fig. 13c) to occupy a significant fraction of the

domain. The detrainment of water substance from the convection contributes to these high relative humidities. When using the ICE-OPT optical properties for ice clouds, the mean visible optical thickness of this cloud layer is close to 0.1. This value is consistent with simulations by a detailed cirrus cloud model of subvisible clouds near the tropopause (Jensen et al. 1996). The single-column model predicts a mean radiative heating of 0.57 K day^{-1} at 100 hPa, the cloud layer being responsible for 0.11 K day^{-1} in this heating. This is consistent with the suggestion of Jensen et al. (1999) that subvisible cirrus increase the radiative heating near the tropopause.

5. Sensitivity of radiative predictions to the main features of the parameterization

The previous section showed some reasonable agreement between satellite data and the radiative fluxes computed by the single-column model including the optimized convection scheme and the cloud parameterization presented in this study. In this section, we investigate the extent to which this agreement depends upon the cloud scheme particularities themselves. Our cloudiness parameterization differs from other statistical cloud schemes currently used in climate models in two main ways: 1) the type of PDF used to describe the subgrid-scale variability of total water, 2) the determination of the variance and the skewness coefficient of this PDF.

The sensitivity of the prediction of the radiative fluxes to the first factor is examined by considering successively a Gaussian PDF (in that case, the only difference with our cloud parameterization is the absence of skewness), a symmetric triangular PDF and a uniform PDF (Table 6). In the two latter cases, the symmetric distribution of q_t is bounded from below and from above, and the half-difference between the minimum and maximum values of q_t is δ. For each PDF, we compute the cloud fraction and the in-cloud water content from (5), (6), and (7), and compute the width of the distribution from (15). Note that the in-cloud water content is independent on the choice of the PDF because the subgrid-scale contribution is predicted directly from the convection scheme and the large-scale contribution from the large-scale variables (of course there is a small feedback of clouds on convection through radiation). The other PDFs uniformly predict slightly larger cloud amounts (by a maximum of 5%–10% in absolute value), and the difference with the generalized lognormal (GNO) PDF increases with height. It was shown in previous sections, indeed, that the skewness of the GNO PDF increases with height. Table 7 shows that the lack of skewness in the PDF (and hence the prediction of larger cloud amounts at upper levels) results, on the average, in a slight reduction of the mean OLR and an enhancement of the mean planetary albedo. However, the day-to-day evolution of the radiative fluxes is very similar (Fig. 14), and the influence upon the rms errors of radiative fluxes is not systematic and of the same order as the uncertainty associated with the representation of cloud optical properties. Although the rms errors are a bit smaller in the case of the GNO PDF, this comparison suggests that the quality of the predicted radiation does not depend critically upon the choice of the PDF.

Another major difference between the present cloudiness parameterization and the other statistical cloud schemes used in climate models is the way the higher-order moments of the q_t distribution are computed. Smith (1990) proposed to compute the variance as a function of the saturation-specific humidity and of a critical RH value, below which the cloud fraction is assumed to be zero.[4] We use critical RH values similar to those used in version 3 of the Hadley Centre model (Pope et al. 2000). Le Treut and Li (1991), on the other hand, proposed to use a uniform PDF of total water and to compute its variance as a function of the mean total water. In these two schemes, the variance is predicted from large-scale variables only, and is not directly related to the subgrid-scale convective activity. Table 6 summarizes these different ways of computing the statistical moments of the total water PDF.

Figure 15 compares the normalized variance of total water predicted for a triangular PDF by using Smith's method or ours, and for a uniform PDF by using Le Treut and Li's method or ours. Both Smith (1990) and Le Treut and Li (1991) methods predict a decreasing variance with altitude (due to the decrease with height of the saturation humidity in the first case, and of the total water in the second case), and predict a normalized variance roughly constant with height in the free troposphere. This is in contrast with our parameterization that predicts an increase of the variance with height (whatever the type of PDF chosen, although the exact amount of variance somewhat depends upon the PDF chosen). A consequence is that above 700 hPa, the two other methods of variance prediction lead to higher (smaller) cloud fractions in supersaturated (subsaturated) environments (due to this compensation, the time-mean cloud amount is very similar for these different methods). On the other hand, they predict a smaller in-cloud water content than our parameterization at most levels in the free troposphere, especially in the upper troposphere.

The radiative impact is shown on Fig. 16. The first-order discrepancies between the observed OLR and planetary albedo and that predicted by the two other schemes are similar to that of our parameterization,

[4] Smith (1990) considered the subgrid-scale variability of both the cloud water and temperature and used a joint symmetric triangular distribution to represent this variability. However, to make the comparison meaningful between the different schemes, we simplify the Smith's scheme by considering only the subgrid-scale variability in total water.

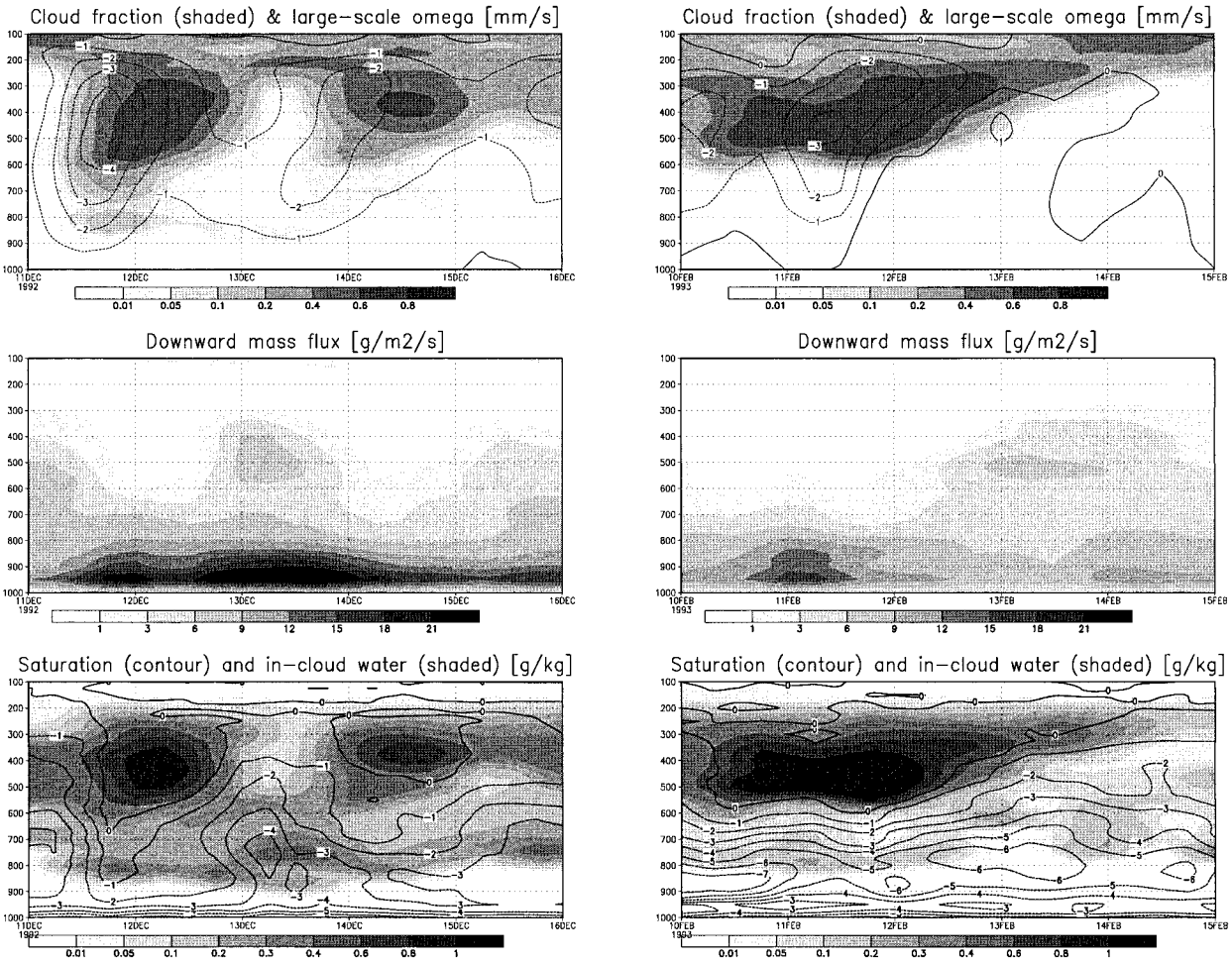

FIG. 12. (upper, shaded) Evolution of the predicted cloud fraction, and (upper, contours) large-scale vertical velocity, (middle) downward mass fluxes, (bottom, shadded) in-cloud water content and (bottom, contours) large-scale saturation ($\overline{q_t} - \overline{q_s}$) over the TOGA COARE IFA during (left) 11–16 Dec 1992 and (right) 10–15 Feb 1993.

whatever the PDF used (cf. Figs. 6 and 16). This suggests that these discrepancies are not specific to the cloud scheme but instead, possibly due to errors in the humidity and temperature profiles used as input to the cloud schemes, and/or in the forcing of the model. On the other hand, when the variance is predicted from large-scale variables only (as it is done in the two other statistical cloud schemes), the contrast between weak and strong convective situations appears to be exaggerated, particularly in the longwave: the radiative impact of clouds is overestimated during episodes of strong convection and underestimated during periods of weak convection. Rms errors of the OLR and planetary albedo are consistently larger when the total water variance is predicted from large-scale variables only, rather than from a combination of large-scale and convective variables (Table 8). A simulation that does not represent any subgrid-scale fractional cloudiness (the cloud fraction and cloud water content are predicted by an all-or-nothing scheme, assuming that the subgrid-scale variance is zero) may provide upper bounds to the rms errors related to the quality of the subgrid-scale cloudiness parameterization. Table 8 shows that the rms errors are less close to these upper bounds when the variance is computed from a combination of large-scale and convective variables, than when it is computed from large-scale variables only. This suggests that the total water variance predicted from large-scale variables only is actually underestimated, and that the approach proposed in this study improves its prediction.

6. Summary and conclusions

This study proposes a new statistical parameterization for use in climate models that predicts the cloudiness (subgrid-scale cloud amount, water content) associated with cumulus convection, and that has been evaluated against TOGA COARE data. The two major characteristics of this PDF-based parameterization is that it is physically coupled with the Emanuel convection

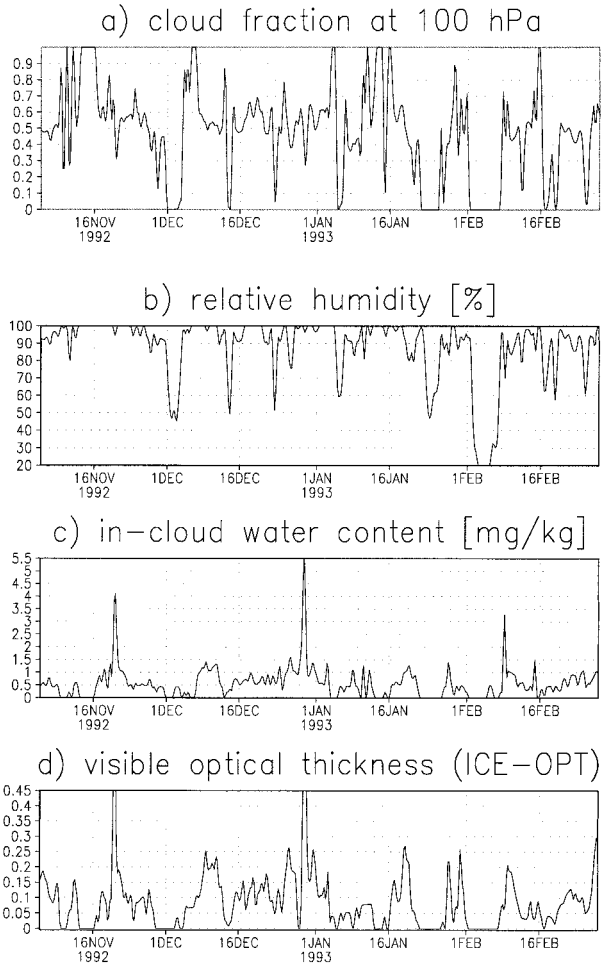

FIG. 13. Time evolution of the cloud fraction, relative humidity, in-cloud water content, predicted at 100 hPa during the 120 days of operation of the TOGA COARE IOP by using a simple representation of cloud optical properties. On the bottom panel, the visible optical thickness at 100 hPa is computed by using a more detailed representation of ice cloud optical properties (ICE-OPT) using an effective radius of 3.5 μm for ice particles at temperatures less than -81.4°C.

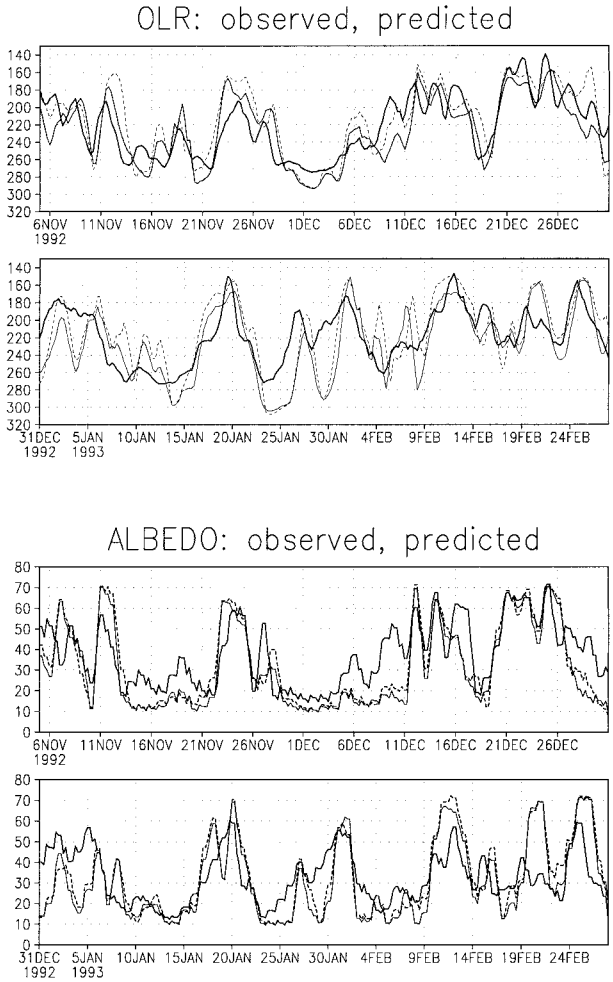

FIG. 14. Comparison of the outgoing longwave radiation (W m^{-2}) and planetary albedo (%) derived from satellite data (thick solid line) and predicted by the single-column model using a generalized lognormal PDF (thin solid line) or a Gaussian PDF (dashed line).

scheme, and that it diagnoses (instead of assumes) the first three statistical moments of the subgrid-scale fluctuations of the total water mixing ratio. The parameterization is based upon the principle that the *local* (in-cloud) concentration of condensed water produced at the subgrid scale is predicted by the parameterization(s) of the subgrid-scale condensation processes itself (here, this is the cumulus convection scheme), and that the statistical cloud scheme predicts how this condensate is spatially distributed within the gridbox. The scheme allows also some cloud condensate to be produced at the large-scale by supersaturation. The domain-averaged cloud water content is then given by the product of the in-cloud water content by the cloud fraction. The in-cloud water content is controlled by the physical processes that produce condensation at the subgrid scale and by the microphysical processes that control the precipitation efficiency. By using it as a predictor of the cloud fraction and of the cloud optical properties, our approach guarantees some consistency between the thermodynamical and radiative effects of clouds.

The main features of the cloudiness parameterization can be summarized as follows.

- The subgrid-scale distribution of the total water mixing ratio is described by a generalized lognormal probability distribution function (PDF) whose variance and skewness coefficients are diagnosed. The diagnostic is based on the amount of condensed water that is produced at the subgrid scale by cumulus convection and at the large scale by supersaturation, the saturation deficit (or excess) of the large-scale environment, and the lower or upper bounds of the total water distribution within the domain. The degree of saturation of the environment naturally depends, among other factors, on the amount of water detrained from the con-

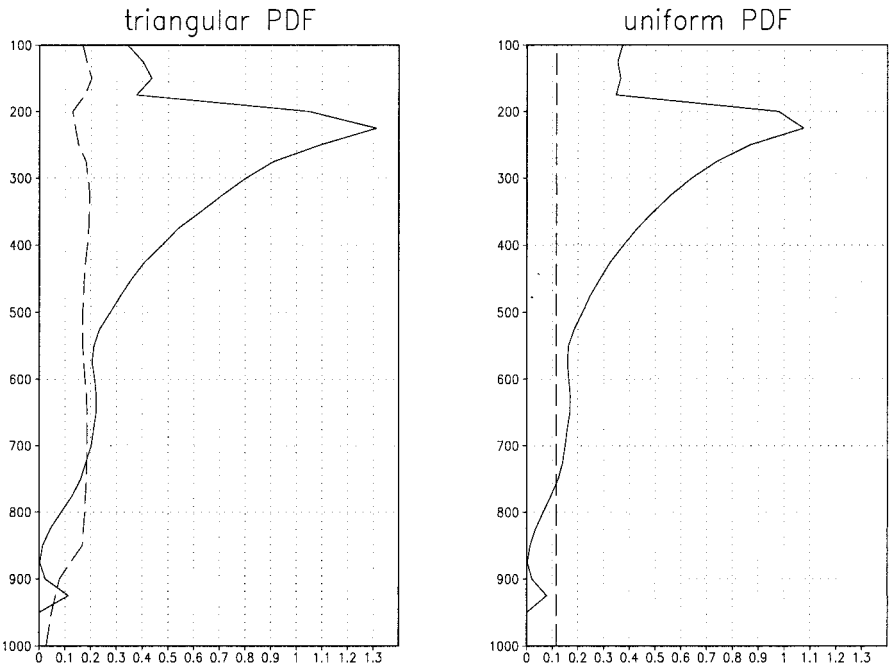

FIG. 15. Comparison of the vertical profile of the total water variance (normalized by the mean total water) predicted (a) for a symmetric triangular PDF following the method proposed by Smith (1990; dashed line) or that proposed in this study (solid line) and (b) for a uniform PDF following the method proposed by Le Treut and Li (1991; dashed line) or that proposed in this study (solid line).

vection. The sign of the skewness coefficient depends on the bounds (lower or upper) on the distribution. By insisting that the total water mixing ratio values are positive, a positive skewness (of variable magnitude) is introduced in the PDF.

- As suggested by CRM simulations of tropical cloud systems, the PDF of the total water mixing ratio is close to a normal distribution at low atmospheric levels and positively skewed at upper levels, and the slope of the relationship between the predicted cloud fraction and the domain-averaged cloud water content gets steeper with altitude.
- If there is no subgrid-scale variability within the domain, the parameterization becomes equivalent to an all-or-nothing large-scale saturation scheme that predicts overcast situations if the environment is saturated, and cloud-free situations if it is subsaturated. In the presence of subgrid-scale condensation, a fractional cloud cover is predicted, even in subsaturated or supersaturated environments.
- The parameterization does not require that any distinction be made between the convective and stratiform cloudiness, and allows one to represent the continuous spectrum of clouds associated with cumulus convection.

The cloudiness parameterization is used in a single-column model forced by TOGA COARE data and including a version of a convection scheme that has been optimized (using these data) in its humidity prediction (EZ99). The model is able to reproduce some of the main characteristics of the cloud systems observed over the warm pool region: the minimum cloud fraction between 600 and 800 hPa; the occurrence of shallow, mid-level, and deep convective clouds; the relationship between the distribution of cloud tops and the presence of stable layers, the formation of long-lasting upper tropospheric anvils associated with the maturation of the convective cloud systems, and the presence of a thin subvisible cirrus cloud layer just below the tropopause.

Radiative fluxes are calculated interactively during the 120 days of operation of the TOGA COARE IOP by using the predicted profiles of temperature, water vapor, cloud fraction, and cloud water content in a radiation code. On average, the OLR and planetary albedo predictions are in reasonable agreement with satellite estimates. However, larger discrepancies occur on a day-to-day basis, due in part to a likely underprediction of shallow-level clouds. By using its own radiative and turbulent fluxes calculated at the surface, the model predicts sea surface temperatures that differ from observations by only a few tenths of a degree. This gives some confidence in the ability of the cloud and convective parameterizations to produce reasonable surface fluxes.

Sensitivity tests show that the performance of the cloud parameterization does not critically depend upon the choice of the PDF, although slightly better radiative predictions are obtained when using a generalized log-

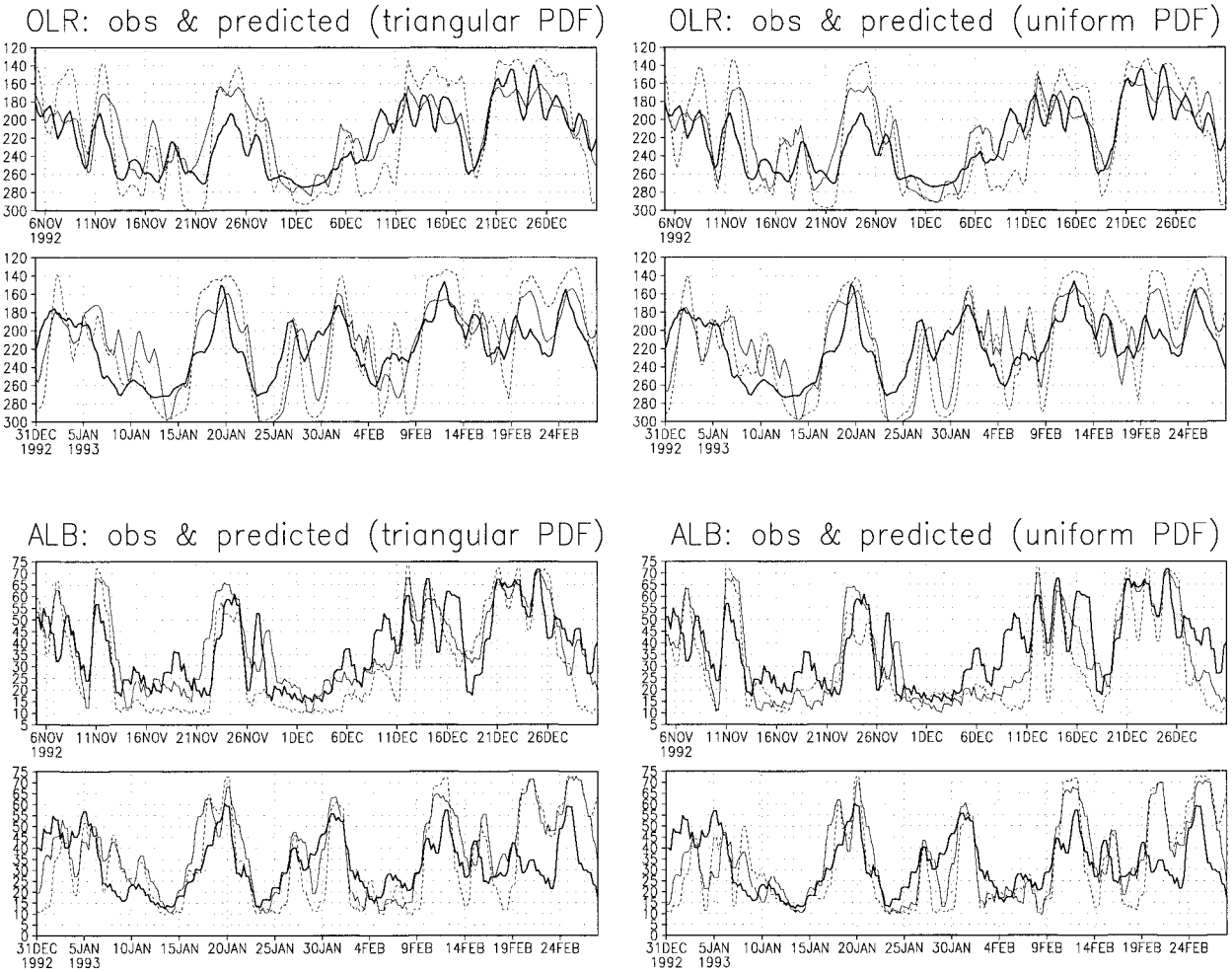

FIG. 16. OLR (W m^{-2}) and planetary albedo (%) observed from satellite during the 120 days of TOGA COARE (thick solid line) and predicted by the single-column model by (a) using a triangular PDF and predicting the total water variance by our method (solid line) or as proposed by Smith (1990; dashed line), (b) a uniform PDF and predicting the total water variance by our method or as proposed by Le Treut and Li (1991; dashed line).

normal PDF (characterized by a variable skewness) instead of symmetric PDFs. On the other hand, it is shown that the prediction of radiative fluxes is improved when the statistical moments of the PDF are predicted from both large-scale variables and subgrid-scale convective activity rather than from large-scale variables only.

It is our intention to evaluate further this coupled cloud-convective parameterization by taking advantage of field experiments that produce measurements of humidity, temperature, wind and surface fluxes, and also clouds. Atmospheric radiation measurements (ARM) datasets will be of primary interest for this purpose. We also intend to use this parameterization in large-scale climate models and address exciting issues such as the role of cloud-radiation interactions in the variability and the sensitivity of tropical climate.

Acknowledgments. This research is supported in part by the Centre National de la Recherche Scientifique (CNRS) and by National Aeronautics and Space Administration (NASA) Grant NAG5-7204 to the Massachusetts Institute of Technology (MIT) as part of the NASA Goddard Institute for Space Studies Interdisciplinary Earth Observation Satellite (EOS) Investigation. We are grateful to Professor P. Stone (MIT) for his support during this study.

APPENDIX A

Generalized Lognormal PDF

This is a modified version of the usual lognormal distribution that includes, within a single PDF, both lognormal distributions with positive skewness and a lower bound, and lognormal distributions with negative skewness and an upper bound, and includes the normal distribution as a special case rather than as an unattainable limit (Hosking and Wallis 1997). It is characterized by

three parameters: λ (location), α (scale), and k (shape) and is defined as follows:

the range of x (in our cloud scheme, x is the total water q_t) is

$$\begin{cases} -\infty < x \leq \lambda + \alpha/k & \text{if } k > 0 \\ -\infty < x < \infty & \text{if } k = 0 \\ \lambda + \alpha/k \leq x < \infty & \text{if } k < 0; \end{cases} \tag{A1}$$

the probability distribution function is

$$P(x) = \frac{e^{ky - y^2/2}}{\alpha\sqrt{2\pi}},$$

$$y = \begin{cases} -\dfrac{1}{k}\ln\left[1 - \dfrac{k(x-\lambda)}{\alpha}\right] & \text{for } k \neq 0 \\ \dfrac{x-\lambda}{\alpha} & \text{for } k = 0; \end{cases} \tag{A2}$$

and the cumulative distribution function ($P(x) = dF(x)/dx$) is;

$$F(x) = \Phi(y) = \int_{-\infty}^{y} \frac{1}{\sqrt{2\pi}} e^{-t^2/2}\, dt, \tag{A3}$$

where Φ is the cumulutative distribution function of the normal distribution.

If X is the lower ($X = \lambda + \alpha/k$, $k < 0$) or upper ($X = \lambda + \alpha/k$, $k > 0$) bound of the distribution $P(x)$, $F(x)$ can also be expressed as

$$F(x) = \frac{1}{2}\left[1 + \text{erf}\left(\frac{-1}{k\sqrt{2}}\ln\left(\frac{X-x}{X-\lambda}\right)\right)\right], \tag{A4}$$

where erf is the error function. It can be shown that the second and third statistical moments of the PDF are given by variance

$$\sigma^2 = (\mu - X)^2(e^{k^2} - 1),$$

and skewness coefficient

$$S = (e^{k^2} + 2)\sqrt{e^{k^2} - 1}\,\frac{\mu - X}{|\mu - X|}.$$

APPENDIX B

Numerical Method Used to Solve σ

If the distribution of the q_t values is bounded by a finite value X (i.e., $k \neq 0$, see appendix A), the value $\tilde{k}$ of k such that equations (13) and (15) are satisfied is found by solving the equation $g(\tilde{k}) = 0$, where $g(k) = (1 - \text{erf}(u))/(1 - \text{erf}(v)) - \beta$ with

$$\begin{cases} u = \dfrac{\gamma}{k\sqrt{2}} + \dfrac{k}{2\sqrt{2}}; & v = \dfrac{\gamma}{k\sqrt{2}} - \dfrac{k}{2\sqrt{2}} \\ \gamma = \ln\left(\dfrac{X-\mu}{X-q_s}\right); & \beta = \dfrac{q_c^{\text{in,SUB}}}{\mu - X} + e^{-\text{MIN}(\gamma,0)}. \end{cases} \tag{B1}$$

As $k \to 0$, the function $g(k)$ may diverge. This may be avoided by considering that the Gaussian limit of the generalized lognormal PDF is reached when $|k| < |\gamma|/\Omega\sqrt{2}$, where Ω is a specified cutoff value for $\gamma/(k\sqrt{2})$, or by using asymptotic expressions of the erf function when $|k| < |\gamma|/\Omega\sqrt{2}$. The results presented in this paper were obtained by using the second method, using $\Omega = 2$.

REFERENCES

Anderson, S. P., R. A. Weller, and R. B. Lukas, 1996: Surface buoyancy forcing and the mixed layer of the western pacific warm pool: Observations and 1D model results. *J. Climate,* **9,** 3056–3085.

Arakawa, A., and W. H. Schubert, 1974: Interaction of a cumulus cloud ensemble with the large-scale environment. *J. Atmos. Sci.,* **31,** 674–701.

Bower, K. N., S. J. Moss, D. W. Johnson, T. W. Choularton, J. Latham, P. R. A. Brown, A. M. Blyth, and J. Cardwell, 1996: A parameterization of the ice water content observed in frontal and convective clouds. *Quart. J. Roy. Meteor. Soc.,* **122,** 1815–1844.

Chen, S. S., and R. A. Houze Jr., 1997: Diurnal variation and lifecycle of deep convective systems over the tropical pacific warm pool. *Quart. J. Roy. Meteor. Soc.,* **123,** 357–388.

——, ——, and B. E. Mapes, 1996: Multiscale variability of deep convection in relation to large-scale circulation in TOGA COARE. *J. Atmos. Sci.,* **53,** 1380–1409.

Chou, S.-H., W. Zhao, and M.-D. Chou, 2000: Surface heat budgets and sea surface temperature in the pacific warm pool during TOGA COARE. *J. Climate,* **13,** 634–649.

Cotton, W. R., and R. A. Anthes, 1989: *Storm and Cloud Dynamics.* International Geophysics Series, Vol. 44, Academic Press, 883 pp.

Del Genio, A. D., M.-S. Yao, W. Kovari, and K. K.-W. Lo, 1996: A prognostic cloud water parameterization for global climate models. *J. Climate,* **9,** 270–304.

Ebert, E. E., and J. A. Curry, 1992: A parameterization of ice cloud optical properties for climate models. *J. Geophys. Res.,* **97,** 3831–3836.

Emanuel, K. A., 1991: A scheme for representing cumulus convection in large-scale models. *J. Atmos. Sci.,* **48,** 2313–2335.

——, and M. Zivkovic-Rothman, 1999: Development and evaluation of a convection scheme for use in climate models. *J. Atmos. Sci.,* **56,** 1766–1782.

Feng, M., P. Hacker, and R. Lukas, 1998: Upper ocean heat and salt balances in response to a westerly wind burst in the western equatorial pacific during TOGA COARE. *J. Geophys. Res.,* **103,** 10 289–10 311.

Fouquart, Y., and B. Bonnel, 1980: Computation of solar heating of the Earth's atmosphere: A new parameterization. *Beitr. Phys. Atmos.,* **53,** 35–62.

Fowler, L. D., and D. A. Randall, 1996: Liquid and ice cloud microphysics in the CSU general circulation model. Part II: Impact on cloudiness, the Earth's radiation budget, and the general circulation of the atmosphere. *J. Climate,* **9,** 489–529.

——, ——, and S. A. Rutledge, 1996: Liquid and ice cloud microphysics in the CSU general circulation model. Part I: Model

description and simulated microphysical processes. *J. Climate*, **9,** 489–529.

Godfrey, J. S., R. A. Houze Jr., R. H. Johnson, R. Lukas, J.-L. Redelsberger, A. Sumi, and R. Weller, 1998: Coupled Ocean-Atmosphere Response Experiment (COARE): An interim report. *J. Geophys. Res.*, **103,** 14 395–14 450.

Heymsfield, A. J., 1986: Ice particles observed in a cirriform cloud at −83°C and implications for polar stratospheric clouds. *J. Atmos. Sci.*, **43,** 851–855.

——, and C. M. R. Platt, 1984: A parameterization of the particle size spectrum of ice clouds in terms of the ambient temperature and the ice water content. *J. Atmos. Sci.*, **41,** 846–855.

——, and G. M. McFarquhar, 1995: Microphysical properties of tropical cirrus anvils. *Proc. Workshop on Cloud Microphysics Parameterizations in Global Atmospheric Circulation Models of the Atmosphere*, Kananaskis, AB, Canada, WMO, 67–80.

——, ——, W. D. Collins, J. A. Goldstein, F. P. J. Valero, J. Spinhirne, W. Hart, and P. Pilewskie, 1998: Cloud properties leading to highly reflective tropical cirrus: Interpretations from CEPEX, TOGA COARE, and Kwajalein, Marshall Islands. *J. Geophys. Res.*, **103,** 8805–8812.

Hosking, J. R. M., and J. R. Wallis, 1997: *Regional Frequency Analysis: An Approach Based on L-Moments.* Cambridge University Press, 224 pp.

Houze, R. A., Jr., and A. K. Betts, 1981: Convection in GATE. *Rev. Geophys. Space Phys.*, **19,** 541–576.

Iacobellis, S. F., and R. C. J. Somerville, 2000: Implications of microphysics for cloud-radiation parameterizations: Lessons from TOGA COARE. *J. Atmos. Sci.*, **57,** 161–183.

Jensen, E. J., O. B. Toon, H. B. Selkirk, J. D. Spinhirne, and M. R. Schoeberl, 1996: On the formation and persistence of subvisible cirrus clouds near the tropical tropopause. *J. Geophys. Res.*, **101,** 21 361–21 375.

——, W. G. Read, J. Mergenthaler, B. J. Sandor, L. Pfister, and A. Tabasadeh, 1999: High humidities and subvisible cirrus near the tropical tropopause. *Geophys. Res. Lett.*, **26,** 2347–2350.

Johnson, R. H., T. M. Rickenbach, S. A. Rutledge, P. E. Ciesielski, and W. H. Schubert, 1999: Trimodal characteristics of tropical convection. *J. Climate*, **12,** 2397–2418.

Kiehl, J. T., and C. S. Zender, 1995: A prognostic ice water scheme for anvil clouds. *Proc. Workshop on Cloud Microphysics Parameterizations in Global Atmospheric Circulation Models of the Atmosphere*, Kananaskis, AB, Canada, WMO, 167–188.

Le Treut, H., and Z.-X. Li, 1991: Sensitivity of an atmospheric general circulation model to prescribed SST changes: Feedback effects associated with the simulation of cloud optical properties. *Climate Dyn.*, **5,** 175–187.

Morcrette, J.-J., 1991: Radiation and cloud radiative properties in the European Centre for Medium-Range Weather Forecasts forecasting system. *J. Geophys. Res.*, **96,** 9121–9132.

Ose, T., 1993: An examination of the effects of explicit cloud water in the UCLA GCM. *J. Meteor. Soc. Japan*, **71,** 93–109.

Pope, V. D., M. R. Gallani, P. R. Rowntree, and R. A. Stratton, 2000: The impact of new physical parameterizations in the Hadley Centre climate model—HadAM3. *Climate Dyn.*, **16,** 123–146.

Randall, D. A., 1989: Cloud parameterization for climate modeling: Status and prospects. *Atmos. Res.*, **23,** 341–361.

Raymond, D. J., and A. M. Blyth, 1986: A stochastic model for nonprecipitating cumulus clouds. *J. Atmos. Sci.*, **43,** 2708–2718.

Slingo, J. M., 1980: A cloud parameterization scheme derived from GATE data for use with a numerical model. *Quart. J. Roy. Meteor. Soc.*, **106,** 747–770.

——, 1987: The development and verification of a cloud prediction scheme for the ECMWF model. *Quart. J. Roy. Meteor. Soc.*, **113,** 899–927.

Smith, R. N. B., 1990: A scheme for predicting layer clouds and their water content in a general circulation model. *Quart. J. Roy. Meteor. Soc.*, **116,** 435–460.

Sommeria, G., and J. W. Deardoff, 1977: Subgrid-scale condensation in models of nonprecipitating clouds. *J. Atmos. Sci.*, **34,** 344–355.

Sud, Y. C., and G. K. Walker, 1999: Microphysics of clouds with the Relaxed Arakawa-Schubert Scheme (McRAS). Part I: Design and evaluation with GATE Phase III data. *J. Atmos. Sci.*, **56,** 3196–3220.

Suzuki, T., M. Tanaka, and T. Nakajima, 1993: The microphysical feedback of cirrus cloud in climate change. *J. Meteor. Soc. Japan*, **71,** 3196–3220.

Tiedtke, M., 1993: Representation of clouds in large-scale models. *Mon. Wea. Rev.*, **121,** 3040–3061.

Wang, P.-H., M. P. McCormick, L. R. Poole, W. P. Chu, G. K. Yue, G. S. Kent, and K. M. Skeens, 1994: Tropical high cloud characteristics derived from SAGE II extinction measurements. *Atmos. Res.*, **34,** 53–83.

Wu, X., W. W. Grabowski, and M. W. Moncrieff, 1998: Long-term behavior of cloud systems in TOGA COARE and their interactions with radiative and surface processes. Part I: Two-dimensional modeling study. *J. Atmos. Sci.*, **55,** 2693–2714.

——, W. D. Hall, W. W. Grabowski, M. W. Moncrieff, W. D. Collins, and J. T. Kiehl, 1999: Long-term behavior of cloud systems in TOGA COARE and their interactions with radiative and surface processes. Part II: Effects of ice microphysics on cloud-radiation interaction. *J. Atmos. Sci.*, **56,** 3177–3195.

Xu, K.-M., and S. K. Krueger, 1991: Evaluation of cloudiness parameterizations using a cumulus ensemble model. *Mon. Wea. Rev.*, **119,** 342–367.

——, and D. A. Randall, 1996a: A semiempirical cloudiness parameterization for use in climate models. *J. Atmos. Sci.*, **53,** 3084–3102.

——, and ——, 1996b: Evaluation of statistically based cloudiness parameterizations used in climate models. *J. Atmos. Sci.*, **53,** 3103–3119.

Zender, C. S., and J. T. Kiehl, 1994: Radiative sensitivities of tropical anvils to small ice crystals. *J. Geophys. Res.*, **99,** 25 869–25 880.

Zhang, Y.-C., W. B. Rossow, and A. A. Lacis, 1999: New radiative transfer model and potential improvements of TOGA surface flux calculation. *Proc. Conf. on the TOGA Coupled Ocean-Atmosphere Response Experiment (COARE)*, Boulder, CO, WMO, 231–232.

Zuidema, P., 1998: On the 600–800-mb minimum in tropical cloudiness. *J. Atmos. Sci.*, **55,** 2220–2228.